Cyclic behavior modeling of a tempered martensitic hot work tool steel

Vincent Velay, Gérard Bernhart, Luc Penazzi

Cyclic Behavior Modeling of a Tempered Martensitic Hot Work Tool Steel

V. Velay [a], G. Bernhart [a,*], L. Penazzi [a]

[a] *Research Centre on Tools, Materials and Processes, École des Mines d'Albi-Carmaux, Route de Teillet, 81013 Albi cedex 9, France*

Abstract

In this paper, a non unified elasto-viscoplastic behavior model based on internal state variables, is investigated in order to describe the thermo-mechanical stress-strain fatigue response of 55NiCrMoV7 tempered martensitic steels (AISI L6). This model considers a quadratic yield criterion to define the elasticity domain. It allows the determination of two inelastic strain mechanisms resulting from two stress states which can be related to the typical continuous cyclic softening of the tempered martensitic steels. This cyclic softening is reproduced through an isotropic component (drag stress). A memory effect is also introduced to take into account the influence of the plastic strain range on the amount of the cyclic softening. The kinematic component (back stress) of the model allows the description of complex load conditions to which tool steels are subjected. Strain recovery (Baushinger effect), time recovery terms (cyclic behavior including tensile dwell times) and ratcheting effects are considered. The numerical implementation is addressed and two integration methods (explicit and implicit) of the constitutive equations are presented. Moreover, the identification methodology of the model parameters from only two sets of experimental data is presented; the coefficients of the kinematic and isotropic parts are determined successively. The main difficulty consists in reaching a good description both of the cyclic behavior for different strain rates and the ratcheting effect. Last, a validation stage of the three dimensional model is investigated from low cycle fatigue tests performed on different notched specimens.

Key words: Tempered martensitic steels, Stress-strain modeling, Constitutive model identification, Numerical simulation

* Corresponding author.
Email address: gerard.bernhart@enstimac.fr (G. Bernhart).

Notations

Tensors

a: Scalar (order 0)	$\overrightarrow{a}$: Vector (order 1)	$\underline{a}$: 2^{nd} order tensor
$\underline{a}^T$: Transpose	$\underline{\underline{a}}$: 4^{th} order tensor	$\underline{\underline{A}}$: 4^{th} order Hooke tensor
$\underline{I}$: 2^{nd} order unit tensor	$\underline{\underline{I}}$: 4^{th} order unit tensor	

Tensor operations and Einstein convention

$x = \overrightarrow{a}.\overrightarrow{b}$	$x = a_i b_i$
$\overrightarrow{x} = \underline{a}\,\overrightarrow{b}$	$x_i = a_{ij} b_j$
$\underline{x} = \underline{\underline{a}}\,\underline{b}$	$x_{ij} = a_{ijkh} b_{kh}$
$\underline{x} = \overrightarrow{a} \otimes \overrightarrow{b}$	$x_{ij} = a_i b_j$
$\underline{\underline{x}} = \underline{a} \otimes \underline{b}$	$x_{ijkh} = a_{ij} b_{kh}$
$x = \underline{a} : \underline{b} = Tr(\underline{a}\,\underline{b})$	$x = a_{ij} b_{ij}$
$\underline{x'} = \underline{x} - \frac{1}{3} Tr(\underline{x}) \underline{I}$	Deviator
$J(\underline{x}) = \sqrt{\frac{3}{2} Tr(\underline{x'}^2)}$	$J(\underline{x}) = \sqrt{\frac{3}{2}(x'_{ij}\ x'_{ij})}$
$< x >= xH(x)$	H is the Heaviside function
$\underline{x} = \frac{\partial a}{\partial \underline{b}}$	$x_{ij} = \frac{\partial a}{\partial b_{ij}}$
$\underline{\underline{x}} = \frac{\partial \underline{a}}{\partial \underline{b}}$	$x_{ijkh} = \frac{\partial a_{ij}}{\partial b_{kh}}$

1 Introduction

Tempered martensitic tool steels are used in forming processes like forging, casting or extrusion for their good mechanical strength at high temperature combined with sufficient ductility. They undergo thermo-mechanical cyclic loads which are very hard to evaluate from an experimental point of view and whose levels strongly depend on the location on the structure. So, numerical simulation seems to be a significant way to reach this information in order to optimize the tools design and to improve their lifetime.

Thus, a good understanding of the martensitic steel behavior is necessary. Materials are subjected to a four stage heat treatment consisting in annealing, austenitizing, followed by a quenching and one or two tempering operations. This treatment leads to a complex micro structure (Delagnes (1998)). The quenching changes the austenite into martensite and the tempering ($560°$ C for the 55NiCrMoV7 steel) gives more ductility to the material. At the end, a thin lath microstructure is observed containing a high dislocation density and carbide precipitates generated respectively by quenching and tempering.

Beside the microstructural aspect, the different kinds of loads induced by the form-

ing process itself have an influence on the behavior. For this purpose, a great variety of approaches were developed since several tenth years. Their complexity strongly depends on the capabilities to describe the various phenomena resulting from the thermo-mechanical loads to which materials are subjected. Three main approaches can be found in the bibliography, the macroscopic, the microscopic and the crystallographic ones.

Macroscopic models are in general divided in two different components (drag and back stresses) able to describe the slow (cyclic hardening or softening) and the fast evolutions of material behavior. Most of time, this approach is in agreement with the irreversible processes of the thermodynamic (Germain and Muller (1995); Halphen and Nguyen (1974); Lemaître and Chaboche (1994); Duvaut (1990); Arnold and Saleeb (1994); Arnold et al. (1995, 1996); Voyiadjis and Al-Rub (2003)). Complexity of the models depends on the investigated phenomena, some of them are unified (Chaboche (1989, 1986); Miller (1976); Schmidt and Miller (1981); Bodner (1987)), other ones are non unified (Blaj and Cailletaud (2000); Cailletaud and Sai (1995); Contesti and Cailletaud (1989)). Both of them allow the description of the strain rate and Baushinger effects. Additional effects can be included in the modeling, like the description of the stress relaxation during a dwell time within a cycle (static or thermal recovery) (Chaboche (1989); Malinin and Khadjinsky (1972); Chan et al. (1988); Yaguchi et al. (2002a,b)). This time dependent effect takes into account a slow recovery of the steel crystalline structure at high temperature by annihilation of dislocations and relaxation of internal stresses, on the one hand, and ratcheting or plastic shakedown effects under stress controlled fatigue tests on the other hand. This requires some changes in the kinematic rule (Gomez (2002); Chaboche (1987); Chaboche et al. (1991); Portier et al. (2000)) or a modification of the yield function (Cailletaud and Sai (1995); Vincent et al. (2004)). Moreover, this last possibility allows to reproduce the inverse rate sensibility resulting from the Portevin-Le Chatelier effect (Abbadi et al. (2002)). Many formulations were developed to describe uniaxial and multi-axial ratcheting and most of them consider a modified kinematic rule (Ohno and Wang (1993); Bari and Hassan (2001, 2000, 2002); Corona et al. (1996); Chen and Jiao (2004); Chen et al. (2005); Döring et al. (2003)). The very important microstructural evolutions which occur when the test temperature exceeds the tempering temperature can be taken into account by an additional variable related to the ageing effect (Nicouleau et al. (2001); Zhang (2002)). The macroscopic approach allows the determination of behavior laws within a validity domain from appropriate low cycle fatigue tests. This approach is able to reproduce very complex thermo-mechanical (Ohno and Wang (1991); Wang and Ohno (1991); Nouailhas et al. (1983); Ben Cheikh (1987); Samrout and Abdi (1997); Yaguchi et al. (2002b)) and nonproportional cyclic loadings (Benallal and Marquis (1987); Colak (2004); Dieng et al. (2005)).

The microscopic approach considers an element scale smaller than 1 μm whereas the macroscopic representative elementary volume is close to 1 mm. However, the internal stress occurring in the two approaches is similar. The microscopic model is based on parameters which can be directly and explicitly related to experimental material microstructural parameters, like dislocation densities, grain sizes (Estrin et al. (1996); Estrin (1996, 1991)).

The last approach concerns the crystallographic models. Nowadays, this way is more and more introduced in structural calculation problems due to the more powerful computers (Forest and Cailletaud (1995); Méric and Cailletaud (1991a,b); Quilici and Cailletaud (1999); Nouailhas et al. (1983, 1995); Flouriot et al. (2003); Cailletaud et al. (2003); Xu and Jiang (2004)) . These models consider a large number of internal variables sometimes one hundred greater than those used in the macroscopic formulations. In this approach, the crystallographic slip is defined as the main mechanism of inelastic strain (Quilici and Cailletaud (1999)). The model formulation is very similar than those of the macroscopic one, but the stress tensor is applied at the grain scale (Eberl et al. (1998)).
Thus, the resolved shear stress can be determined for each system (Schmid law). In this paper, an intermediate approach between the macroscopic and the crystallographic ones is considered. It is based on the non unified model developed by Cailletaud and Sai (1995) and allows to take into account in a macroscopic frame two different inelastic strain mechanisms; such model seems well adapted to describe the microstructural specificities of the tempered martensitic steels for which two softening mechanisms were clearly identified (Mébarki (2003); Zhang (2002)). After a presentation of the experimental behavior under cyclic conditions, the 2M1C (Two Mechanisms and one yield Criterion) model and its numerical implementation are presented. Identification methodology and numerical simulation validation are performed on notched samples under cyclic loadings.

2 Behavior of the 55NiCrMoV7 steel

This section deals with the experimental behavior of the 55NiCrMoV7 steel, it describes in detail the specific fatigue tests able to determine completely the model parameters.

2.1 Experimental equipment and material investigated

The low cycle fatigue tests were carried out with a MTS servo-hydraulic testing machine and Testar II™ controller connected to a computer. Heating was achieved with an induction coil. A more detailed description of the experimental setup can be found in Zhang et al. (2002).

The 42 HRc (Rockwell hardness) 55NiCrMoV7 martensitic steel is investigated in isothermal fatigue conditions for a temperature range between $20° C$ and $500° C$. The continuous softening from the first cycle until rupture is typical of such materials. If the stress amplitude is plotted versus the number of cycles, this softening can be divided in three successive stages (see figure 1).

Indeed, the strong softening stage occurring during the first hundred cycles is followed by a pseudo-stability one (weak softening) during the major part of the life-

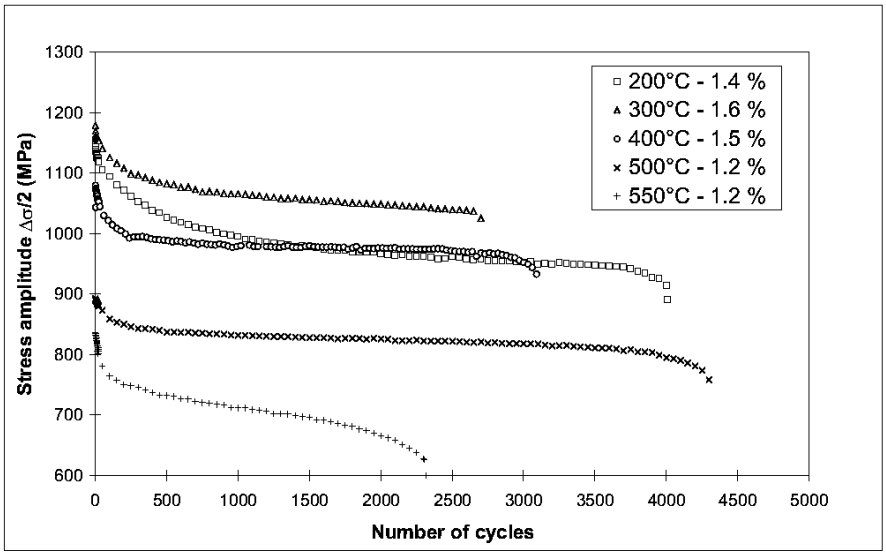

Figure 1. Cyclic softening of the 55NiCrMoV7 steel Bernhart et al. (1999)

time. At the end, crack propagation occurs, defined by a fast decrease of the stress amplitude before the rupture (Bernhart et al. (1999)).

The chemical composition of the steel is presented in the table 1, and the heat treatment operations are described in the table 2.

Table 1
Chemical composition of the $55NiCrMoV7$ steel (% in weight)

Elements	C	Ni	Cr	Mo	V	Si	Mn	Fe
55NiCrMoV7	0.56	1.70	1.10	0.50	0.10	0.20	0.70	bal

Table 2
Heat treatment operations of the $55NiCrMoV7$ steel

Steel	Austenitizing	Quenching	Tempering	Hardness
55NiCrMoV7	875° C	1h/oil	560° C/2h	42 HRc

2.2 Fatigue testing procedure

Two types of cyclic tests are performed in order to identify the model parameters for the temperatures 20, 300, 400 and 500° C. The first one (type I, see figure 2) may be divided in two different steps:

- the first step is a symmetrical total strain controlled push-pull low cycle fatigue test, with a fixed strain range $\Delta\varepsilon_t = 1.6\%$, itself divided in three sub-steps.

- Sub-step 1 consists in a number of fatigue cycles so as to reach a cumulative plastic strain p close to 4 at a constant strain rate of $10^{-2}s^{-1}$. This part is illustrated on Figure 3 for different temperature levels.

- During the sub-step 2, strain rate is varied from 10^{-2} to 10^{-3} and $10^{-4}s^{-1}$; and three cycles are performed at each strain rate (see figure 4 for a temperature of $500°\ C$).

- At last, fatigue relaxation cycles are included with a strain rate of $10^{-2}s^{-1}$ and where relaxation time is varied from $30s$ (3 cycles) to $90s$ and $600s$ (2 cycles for each one). An example of fatigue relaxation loops is plotted on figure 5 for a temperature of $500°\ C$.

- the second step consists in a non-symmetrical stress controlled fatigue test at a constant stress rate of $100MPa.s^{-1}$. Ten cycles are performed.

Each test performed can be related to typical loads induced by the industrial hot forming processes. Indeed, the high strain rates (about $10^{-2}s^{-1}$) is intended to reproduce those induced in the mechanical forging or casting industry, whereas the low strain rates (about $10^{-4}s^{-1}$) to take into account those of the hydraulic forging. The dwell times included in the fatigue loops are requested to describe the extrusion processes. Last, the behavior can be influenced by the types of loading. Indeed, depending on the stress amplitude applied, a stress controlled test leads to a progressive strain increase. The stress amplitude applied can induce a stabilization (plastic shakedown, see figure 6) or an increase of the cyclic strain (ratcheting, see figure 7). These typical cycles can be induced in some hot forming processes due to structural effects. The stress levels applied are summed up in the table 3.

Some examples of the second kind of test (Test II) performed are illustrated on figure 8 for different levels of temperature. It consists in a symmetrical total strain fatigue test at constant strain rate of $10^{-2}s^{-1}$, in which strain range is varied from ± 0.6, to ± 0.7, ± 0.8 and ± 0.9 before to coming back to $\pm 0.7\%$. The number of cycles is selected so as to reach a cumulative plastic strain p close to 1 for each strain range applied.

Table 3
Stress range levels $\Delta\sigma$ (MPa) of the stress controlled fatigue tests

Temperature [$°\ C$]	20	300	400	500
55NiCrMoV7	-500/1000	-480/960	-470/940	-450/900

The characteristic values (see table 4) of a hysteresis loop can be extracted from the experimental data. These values are compared with those provided by the behavior model.

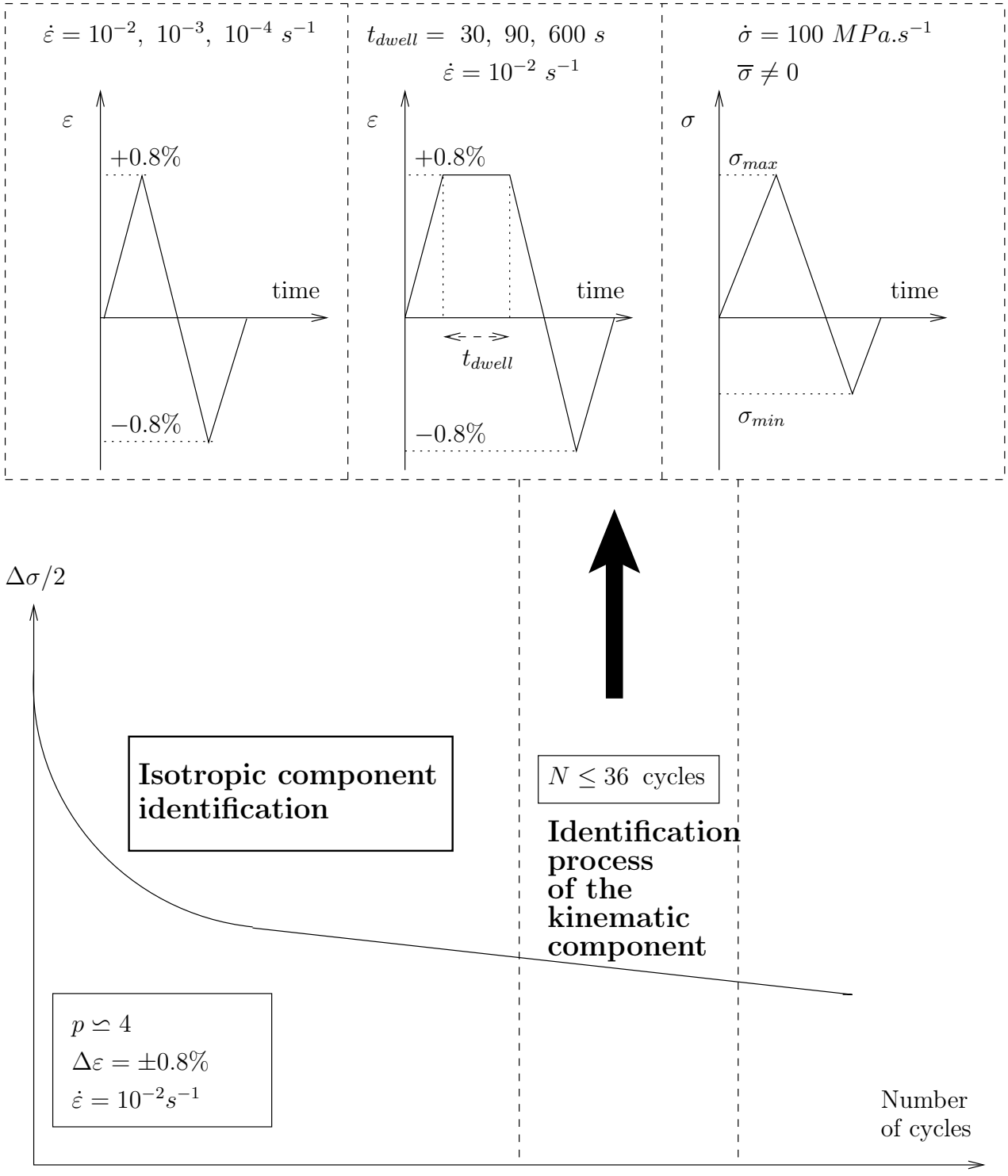

Figure 2. Type I test and related identification methodology

For each kind of tests (Type I and II), time, temperature, strength, displacement, strain and stress are registered for the twenty first cycles, then all the ten cycles for the strain rate of $10^{-2}s{-}1$. For the end of the test including different strain rates, dwell times and stress controlled loads, all the cycles are registered. An automatic process allows to extract the experimental files, to calculate the Young modulus and to plot the $\sigma - \varepsilon_p$ or $\Delta\sigma/2 - p$ curves for each fatigue test.

Table 4
Characteristic values of a hysteresis loop

$\Delta\varepsilon = \varepsilon_{max} - \varepsilon_{min}$	Strain range
$\Delta\varepsilon_p = \varepsilon^i_{pmax} - \varepsilon^i_{pmin}$	Plastic strain range at the i^{th} cycle
$\Delta\sigma = \sigma^i_{max} - \sigma^i_{min}$	Stress range at the i^{th} cycle
$p = \sum_{i=1}^{N} 2\Delta\varepsilon^i_p$	Cumulative plastic strain at the Nth cycle
$\delta\sigma = (\Delta\sigma/2)_{max} - (\Delta\sigma/2)_{min}$	Cyclic softening amplitude

2.3 Test results

The test temperature has a great impact on the behavior. First, the cyclic softening amplitude decreases with the temperature, then increases from the temperature of 300° C to 500° C. Moreover, the linear part of the softening is not influenced by the temperature (see figure 3). The different strain level tests allow to take into account the memory effect of plastic strain path history. Thus, after several cycles leading to the linear part of the softening, an increase of the strain amplitude implies a new strong softening. On the contrary, a decrease of this amplitude provides a linear softening (see figure 8).

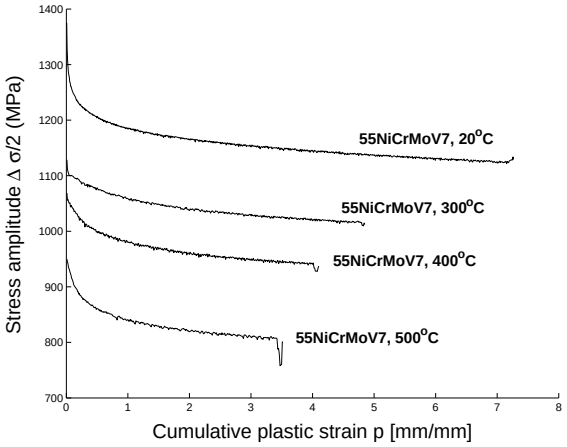

Figure 3. Cyclic softening with a constant strain range ($\Delta\varepsilon/2 = \pm 0.8\%$)

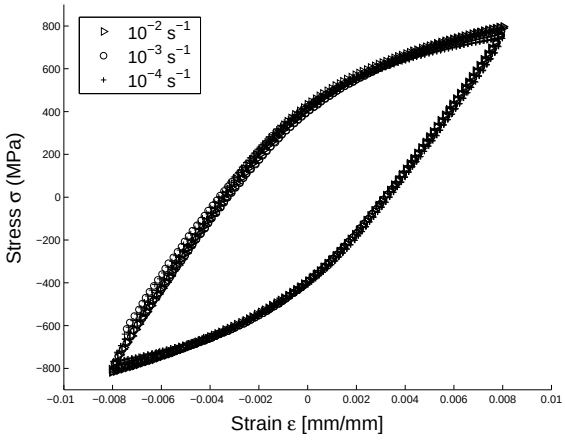

Figure 4. Strain controlled fatigue tests with different strain rates for a temperature of 500° C

The strain rate effect is shown in figure 4 where stress-strain loops at three strain rates $10^{-2}s^{-1}$, $10^{-3}s^{-1}$, $10^{-4}s^{-1}$, for a temperature of 500° C are plotted. The dwell effect is also a time dependent effect which is activated with the temperature. Indeed the stress relaxation during the dwell time is increased when dwell time increases.

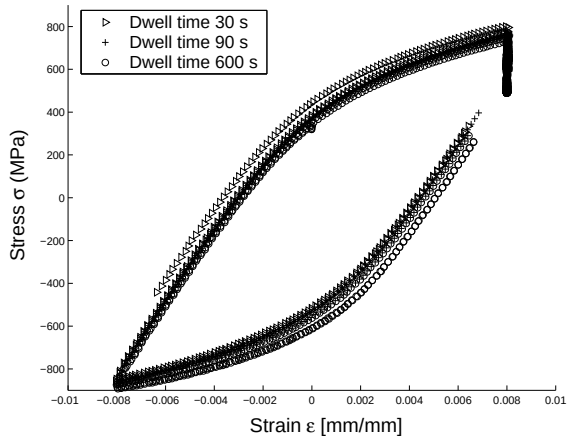

Figure 5. Strain controlled fatigue tests including different dwell times for a temperature of 500° C

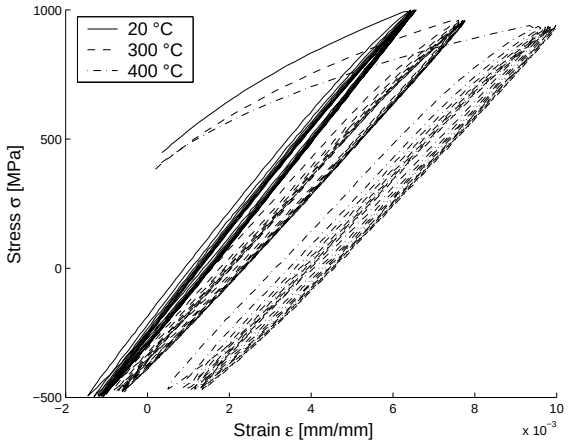

Figure 6. Stress controlled fatigue tests for different levels of temperature

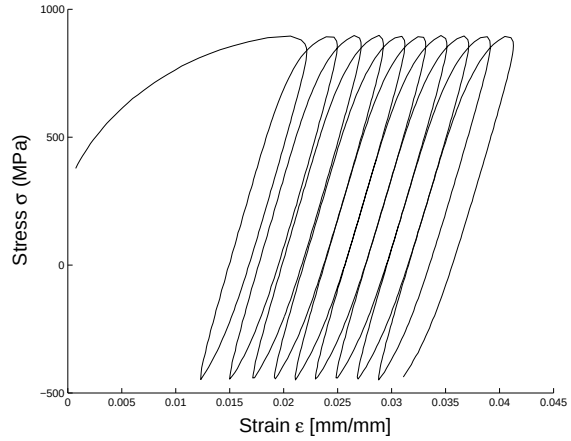

Figure 7. Stress controlled fatigue test for a temperature of 500° C

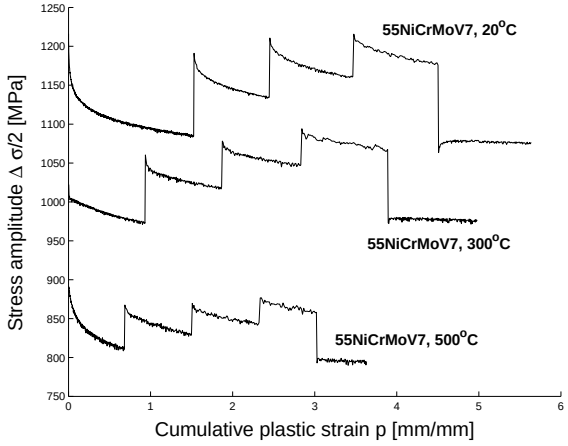

Figure 8. Cyclic softening with different strain ranges

3 Behavior Modeling

The model formulation intended to take into account the previous experimental features is presented in detail in the following. Basic assumptions are small strains and isotropic elastoviscoplastic behavior.

Numerical implementation and Jacobian matrix calculation are also detailed.

3.1 Investigation of the 2 mechanisms - 1 yield criterion (2M1C) model

First, thermodynamic framework, state laws and evolution equations of the $2M1C$ behavior model (Cailletaud and Sai (1995)) are presented.

3.1.1 Free Energy Potential and state laws

The free energy potential can be written:

$$\rho\Psi = \rho\Psi_e + \rho\Psi_{in} = \rho\Psi_e(\underline{\varepsilon_e}, T) + \rho\Psi_{in}(\underline{\alpha_i}, q_i, T)$$

Its thermo-elastic part has the following form:

$$\rho\Psi_e = \tfrac{1}{2}\underline{\underline{A}}\underline{\varepsilon_e} : \underline{\varepsilon_e} + \underline{M}(T) : \underline{\varepsilon_e}$$

with:

$$\left(\underline{\underline{A}}(T)\right)_{ijkh} = \tfrac{\nu E(T)}{(1-2\nu)(1+\nu)}\delta_{ij}\delta_{kh} + \tfrac{E(T)}{2(1+\nu)}(\delta_{ik}\delta_{jh} + \delta_{ih}\delta_{jk})$$

$$\underline{M}(T) = -\tfrac{E(T)}{1-2\nu}\alpha_{th}\Delta T\underline{I}$$

$\Delta T = T - T_0$ with T_0 the absolute temperature

E is the Young modulus and ν the Poisson ratio

Total strain is partitioned in an elastic and inelastic components. In the 2M1C formulation, inelastic strain can be partitioned itself in two different strain mechanisms.

$$\underline{\varepsilon} = \underline{\varepsilon_e} + \underline{\varepsilon_{in}}; \qquad \underline{\varepsilon_{in}} = A_1\underline{\varepsilon_1} + A_2\underline{\varepsilon_2}$$

Each strain mechanism is associated to a stress state resulting from the free energy potential. The terms linked to the thermal part of the stress tensor will not be considered in the following expressions.

$$\underline{\sigma} = \rho\tfrac{\partial\Psi}{\partial\underline{\varepsilon_e}} = \underline{\underline{A}}\ \underline{\varepsilon_e} = \tfrac{\nu E}{(1-2\nu)(1+\nu)}tr(\underline{\varepsilon_e})\underline{I} + \tfrac{E}{1+\nu}\underline{\varepsilon_e} - \tfrac{E}{1-2\nu}\alpha_{th}\Delta T\underline{I}$$

$$\underline{\sigma_1} = -\rho\tfrac{\partial\Psi}{\partial\underline{\varepsilon_1}} = -\rho\tfrac{\partial\underline{\varepsilon_e}}{\partial\underline{\varepsilon_1}}\tfrac{\partial\Psi}{\partial\underline{\varepsilon_e}} = -\tfrac{\partial}{\partial\underline{\varepsilon_1}}(\underline{\varepsilon} - \underline{\varepsilon_{in}})\underline{\underline{A}}\ \underline{\varepsilon_e} = \tfrac{\partial\underline{\varepsilon_{in}}}{\partial\underline{\varepsilon_1}}\underline{\underline{A}}\ \underline{\varepsilon_e} = A_1\underline{\underline{A}}\ \underline{\varepsilon_e} = A_1\underline{\sigma}$$

And: $\underline{\sigma_2} = A_2\underline{\sigma}$

The inelastic part of the free energy induces the definition of different state coupling (kinematic-kinematic, kinematic-isotropic, isotropic-isotropic) which could be related by several mechanisms for example as a low and a high dislocation density (Blaj and Cailletaud (2000)).

$$\rho\Psi_{in} = \tfrac{1}{3}(\underline{\alpha_1} \quad \underline{\alpha_2}) \begin{pmatrix} C_{11} & C_{12} \\ C_{12} & C_{22} \end{pmatrix} \begin{pmatrix} \underline{\alpha_1} \\ \underline{\alpha_2} \end{pmatrix} + \tfrac{1}{2}(q_1 \quad q_2) \begin{pmatrix} b_{11}Q_{11} & b_{12}Q_{12} \\ b_{12}Q_{12} & b_{22}Q_{22} \end{pmatrix} \begin{pmatrix} q_1 \\ q_2 \end{pmatrix}$$

which implies:

$$\rho\Psi_{in} = \frac{1}{3}\Big(C_{11}\underline{\alpha_1}^2 + 2C_{12}\underline{\alpha_1}\underline{\alpha_2} + C_{22}\underline{\alpha_2}^2\Big) + \frac{1}{2}\Big(b_{11}Q_{11}q_1^2 + b_{22}Q_{22}q_2^2 + 2b_{12}Q_{12}q_1q_2\Big)$$

Thus:

$$\underline{X_1} = \rho\frac{\partial\Psi}{\partial\underline{\alpha_1}} = \frac{2}{3}\Big(C_{11}\underline{\alpha_1} + C_{12}\underline{\alpha_2}\Big); \qquad \underline{X_2} = \rho\frac{\partial\Psi}{\partial\underline{\alpha_2}} = \frac{2}{3}\Big(C_{22}\underline{\alpha_2} + C_{12}\underline{\alpha_1}\Big) \tag{1}$$

If no coupling is considered for the isotropic variable, $Q_{12} = 0$

$$R_1 = \rho\frac{\partial\Psi}{\partial q_1} = b_{11}Q_{11}q_1; \qquad R_2 = \rho\frac{\partial\Psi}{\partial q_2} = b_{22}Q_{22}q_2 \tag{2}$$

Note following notations: $b_{11} = b_1$; $\quad b_{22} = b_2$; $\quad Q_{11} = Q_1$; $\quad Q_{22} = Q_2$.

3.1.2 Evolution equations

The quadratic yield criterion is a function of the local stresses $\underline{\sigma_i}$ related to the two inelastic mechanisms $\underline{\varepsilon_i}$ $\quad i = 1, 2$.

$$f = \sqrt{J(\underline{\sigma_1} - \underline{X_1})^2 + J(\underline{\sigma_2} - \underline{X_2})^2} - R_1 - R_2 - R_0$$

This yield criterion as the classical Von Mises yield criterion depends on the state variables $(\underline{\sigma_i}, \underline{X_i}, R_i)$. In order to allow the introduction of the dynamic recovery terms and the non linear isotropic variables, additional terms, depending on internal variables $(\underline{\alpha_i}, q_i)$ and considered as parameters, can be added (Lemaître and Chaboche (1994)). These extra terms vanishe using the state laws. Thus, the yield function can be written as:

$$f(\underline{\sigma_i}, \underline{X_i}, R_i; \underline{\alpha_i}, q_i) = f + \frac{R_1^2}{2Q_1} + \frac{R_2^2}{2Q_2} + \frac{3}{4}\frac{D_1}{C_{11}}\underline{X_1} : \underline{X_1} + \frac{3}{4}\frac{D_2}{C_{22}}\underline{X_2} : \underline{X_2} - \frac{b_1^2Q_1}{2}q_1^2 - \frac{b_2^2Q_2}{2}q_2^2$$
$$-\frac{1}{3}\Big(C_{11}^2\underline{\alpha_1} : \underline{\alpha_1} + C_{22}^2\underline{\alpha_2} : \underline{\alpha_2} + C_{12}^2(\underline{\alpha_1} : \underline{\alpha_1} + \underline{\alpha_2} : \underline{\alpha_2}) + 2C_{12}(\underline{\alpha_1} + \underline{\alpha_2})(C_{11} + C_{22})\Big)$$

Dissipation potential can be written as:

$$\Omega = \Omega_{vp}(f) + \Omega_R$$

With:

$$\Omega_R = \sum_{k=1}^{2}\frac{M_k}{m_k+1}\left\langle\frac{J(\underline{X_k})}{M_k}\right\rangle^{m_k+1} \quad \text{et} \quad \Omega_{vp}(\underline{\sigma}, \underline{X_i}, R_i; \underline{\alpha_i}, q_i) = \frac{K}{n+1}\left\langle\frac{f}{K}\right\rangle^{n+1}; \quad i = 1, 2$$

Evolution equations have the following forms:

$$\underline{\dot{\varepsilon_1}} = \frac{\partial \Omega}{\partial \underline{\sigma_1}} = \frac{\partial \Omega_{vp}(f)}{\partial \underline{\sigma_1}} = \Omega_{vp}{}'(f)\frac{\partial f}{\partial \underline{\sigma_1}}$$
$$= \frac{3}{2}\left\langle \frac{f}{K} \right\rangle^n \frac{\underline{\sigma_1'} - \underline{X_1'}}{\sqrt{J(\underline{\sigma_1} - \underline{X_1})^2 + J(\underline{\sigma_2} - \underline{X_2})^2}}$$

Thus:

$$\underline{\dot{\varepsilon_1}} = \frac{3}{2}\dot{\lambda}\frac{\underline{\sigma_1'} - \underline{X_1'}}{\sqrt{J(\underline{\sigma_1} - \underline{X_1})^2 + J(\underline{\sigma_2} - \underline{X_2})^2}} = \dot{\lambda}\underline{n_1}$$

and:

$$\underline{\dot{\varepsilon_2}} = \frac{3}{2}\dot{\lambda}\frac{\underline{\sigma_2'} - \underline{X_2'}}{\sqrt{J(\underline{\sigma_1} - \underline{X_1})^2 + J(\underline{\sigma_2} - \underline{X_2})^2}} = \dot{\lambda}\underline{n_2}$$

with: $\underline{n_i} = \frac{\partial f}{\partial \underline{\sigma_i}}$; i=1;2.

Note that:

$$\sqrt{\frac{2}{3}(\underline{\dot{\varepsilon_1}} : \underline{\dot{\varepsilon_1}} + \underline{\dot{\varepsilon_2}} : \underline{\dot{\varepsilon_2}})} = \left\langle \frac{f}{K} \right\rangle^n = \dot{\lambda} \neq \dot{p}; \qquad \dot{p} = \sqrt{\frac{2}{3}\underline{\dot{\varepsilon_{in}}} : \underline{\dot{\varepsilon_{in}}}}$$

Moreover:

$$\underline{\dot{\alpha_1}} = -\frac{\partial \Omega}{\partial \underline{X_1}} = -\frac{\partial \Omega_{vp}(f)}{\partial X_1} - \frac{\partial \Omega_R}{\partial \underline{X_1}} = -\Omega'_{vp}(f)\frac{\partial f}{\partial \underline{X_1}} - \frac{\partial \Omega_R}{\partial \underline{X_1}}$$
$$= \frac{3}{2}\dot{\lambda}\left(\frac{\underline{\sigma_1'} - \underline{X_1'}}{\sqrt{J(\underline{\sigma_1} - \underline{X_1})^2 + J(\underline{\sigma_2} - \underline{X_2})^2}} - \frac{D_1}{C_{11}}\underline{X_1}\right) - \frac{3}{2}\frac{\underline{X_1}}{J(\underline{X_1})}\left\langle \frac{J(\underline{X_1})}{M_1} \right\rangle^{m_1}$$

Finally, internal variable evolution equations are:

$$\begin{aligned} \underline{\dot{\alpha_1}} &= \underline{\dot{\varepsilon_1}} - \frac{3}{2}\dot{\lambda}\frac{D_1}{C_{11}}\underline{X_1} - \frac{3}{2}\frac{\underline{X_1}}{J(\underline{X_1})}\left\langle \frac{J(\underline{X_1})}{M_1} \right\rangle^{m_1}; \\ \underline{\dot{\alpha_2}} &= \underline{\dot{\varepsilon_2}} - \frac{3}{2}\dot{\lambda}\frac{D_2}{C_{22}}\underline{X_2} - \frac{3}{2}\frac{\underline{X_2}}{J(\underline{X_2})}\left\langle \frac{J(\underline{X_2})}{M_2} \right\rangle^{m_2} \end{aligned} \tag{3}$$

and:

$$\dot{q_1} = -\frac{\partial \Omega}{\partial R_1} = \dot{\lambda}(1 - \frac{R_1}{Q_1}); \qquad \dot{q_2} = -\frac{\partial \Omega}{\partial R_2} = \dot{\lambda}(1 - \frac{R_2}{Q_2}) \tag{4}$$

3.1.3 Intrinsic dissipation

Model is in agreement with the thermodynamic principles if intrinsic dissipation is positive.

In this case, it is written:

$$\mathcal{D}_{int} = \underline{\sigma} : \underline{\dot{\varepsilon_{in}}} - R_1\dot{q_1} - R_2\dot{q_2} - \underline{X_1} : \underline{\dot{\alpha_1}} - \underline{X_2} : \underline{\dot{\alpha_2}}$$
$$= \underline{\sigma_1} : \underline{\dot{\varepsilon_1}} + \underline{\sigma_2} : \underline{\dot{\varepsilon_2}} - R_1\dot{q_1} - R_2\dot{q_2} - \underline{X_1} : \underline{\dot{\alpha_1}} - \underline{X_2} : \underline{\dot{\alpha_2}}$$

which can be formulated:

$$\mathcal{D}_{int} = \dot{\lambda}\left(f + R_0 + \frac{R_1^2}{Q_1} + \frac{R_2^2}{Q_2}\right) + \sum_{i=1}^{2} \frac{3}{2}\dot{\lambda}\frac{Di}{C_{ii}}\underline{X_i}^2 + J(\underline{X_i})\left\langle\frac{J(X_i)}{M_i}\right\rangle^{m_i} \geq 0$$

This expression is always positive.

3.1.4 Memory effect of the strain range

The memory effect, first introduced by Chaboche (1986); Chaboche et al. (1979), is considered on the global inelastic strain $\underline{\varepsilon_{in}} = A_1\underline{\varepsilon_1} + A_2\underline{\varepsilon_2}$ through the asymptotic value Q_1 of the isotropic variable R_1 describing the strong softening. So, the asymptotic value Q_1 changes when the inelastic strain exceeds a threshold F which is called non hardening region (Chaboche (1986); Chaboche et al. (1979)). The unit normals $\underline{n}$ to the yield surface and $\underline{n^*}$ to the non hardening region are calculated from the expression of the yield criterion.

$$\begin{aligned}
&F = \tfrac{2}{3}J(\underline{\varepsilon_p} - \underline{\xi}) - q \\
&\dot{q} = \eta H(F)\langle\underline{n} : \underline{n^*}\rangle\dot{p} \\
&\underline{\dot{\xi}} = \sqrt{\tfrac{3}{2}}(1-\eta)H(F)\langle\underline{n} : \underline{n^*}\rangle\underline{n^*}\dot{p} \\
&\underline{n^*} = \frac{\partial F}{\partial\underline{\varepsilon_p}}/|\frac{\partial F}{\partial\underline{\varepsilon_p}}| = \sqrt{\tfrac{3}{2}}\frac{\underline{\varepsilon_p}' - \underline{\xi}'}{J(\underline{\varepsilon_p} - \underline{\xi})} \\
&\underline{n} = \frac{\frac{\partial f}{\partial\underline{\sigma}}}{||\frac{\partial f}{\partial\underline{\sigma}}||} = \frac{\sqrt{\frac{3}{2}}\left(A_1\left(\underline{\sigma_1'} - \underline{X_1'}\right) + A_2\left(\underline{\sigma_2'} - \underline{X_2'}\right)\right)}{\sqrt{A_1^2 J\left(\underline{\sigma_1} - \underline{X_1}\right)^2 + A_2^2 J\left(\underline{\sigma_2} - \underline{X_2}\right)^2 + 3A_1A_2\left(\underline{\sigma_1}' - \underline{X_1'}\right):\left(\underline{\sigma_2'} - \underline{X_2'}\right)}}
\end{aligned} \tag{5}$$

With:

$$\frac{\partial f}{\partial\underline{\sigma}} = \frac{3}{2}\frac{A_1(\underline{\sigma_1}' - \underline{X_1}') + A_2(\underline{\sigma_2}' - \underline{X_2}')}{\sqrt{J(\underline{\sigma_1} - \underline{X_1})^2 + J(\underline{\sigma_2} - \underline{X_2})^2}}$$

$$||\frac{\partial f}{\partial\underline{\sigma}}|| = \sqrt{\frac{3}{2}}\sqrt{\frac{A_1^2 J(\underline{\sigma_1} - \underline{X_1})^2 + A_2^2 J(\underline{\sigma_2} - \underline{X_2})^2 + 3A_1A_2(\underline{\sigma_1}' - \underline{X_1}'):(\underline{\sigma_2}' - \underline{X_2}')}{J(\underline{\sigma_1} - \underline{X_1})^2 + J(\underline{\sigma_2} - \underline{X_2})^2}}$$

The asymptotic value Q_1 takes the follwing form:

$$Q_1 = Q_{1\infty}.(1 - e^{-2\mu q})$$

Note that this effect can not be included in the thermodynamic framework introduced previously. In fact, the memory varibles q and $\underline{\xi}$ are not considered as state variables but they are chosen as parameters in the dissipation potential.

3.1.5 Conclusion

Table 5 presents all the $2M1C$ thermodynamic variables.

Table 5
Thermodynamic variables of the $2M1C$ model

Observable variable	Internal variables	Associated variables
$\underline{\varepsilon}$		$\underline{\sigma}$
	$\underline{\varepsilon_e}$	$\underline{\sigma}$
	$\underline{\varepsilon_1}$	$-\underline{\sigma_1}$
	$\underline{\varepsilon_2}$	$-\underline{\sigma_2}$
	$\underline{\alpha_i}$	$\underline{X_i}$ $i = 1, 2$
	q_i	R_i $i = 1, 2$

Table 6 shows the 19 model parameters which have to be identified.

Table 6
2M1C model coefficients

E R_0	Young modulus and true elasticity limit
K n	Viscous coefficients
C_{11} C_{22} C_{12}	Parameters of the kinematic part
D_1 D_2	Dynamic recovery terms
A_1 A_2	Localization coefficients of the strain mechanisms
M_1 M_2 m_1 m_2	Static recovery terms
$Q_{1\infty}$ Q_2 b_1 b_2	Parameters of the isotropic part

Following previous work (Zhang et al. (2002)), the memory parameters μ is taken equal to 420 for all the temperature levels. Moreover, if only symmetrical strain controlled tests are considered, η equals 0.5 (instantaneous memorization), in the other cases, η equals 0.1 for progressive memorization (Chaboche (1986); Nouailhas et al. (1983); Ohno (1982); Zhang (2002)).

3.2 Numerical Implementation

Implementation of the model in a finite element code requires some developments which are addressed in the following. Numerous authors (Foerch (1996); Foerch et al. (2000); Lemaître et al. (1992); Simo and Taylor (1985); Alfano et al. (2001); Abdel-Karim (2004); Voyiadjis et al. (2004)) have published works on this matter. In the structural calculation, the constitutive equations are evaluated at each Gauss integration point in order to simulate the material behavior. The finite element approximation of the elasto-viscoplastic problems leads to:

- on the one hand, $\underline{K}\,\overrightarrow{u} = \overrightarrow{F}$.
  $\underline{K}$ is the global stiffness matrix, $\overrightarrow{u}$ the node displacements and $\overrightarrow{F}$ the external loads.
- on the other hand, the equilibrium equations are combined to the local integration of the constitutive model equations within each element.

So, the numerical integration methods allow to solve the equilibrium equations (global method) and the constitutive equations (local integration algorithms) depending on the software used (Benallal (1990)). In this investigation, the equilibrium equations are solved with the ABAQUS™ software whereas the Z-Front tool box of the Zebulon™ software (Zset package (1996)) allows integration of the constitutive equations of the model. Two local methods are available:

- explicit Runge Kutta method
- implicit θ-method which need the calculation of the constitutive model Jacobian matrix

Residual and Jacobian matrixes

$\underline{R_e} = \Delta\underline{\varepsilon_e} - \Delta\underline{\varepsilon_t} + \Delta\underline{\varepsilon_{in}} = \Delta\underline{\varepsilon_e} - \Delta\underline{\varepsilon_t} + A_1\Delta\underline{\varepsilon_1} + A_2\underline{\varepsilon_2} = \Delta\underline{\varepsilon_e} - \Delta\underline{\varepsilon_t} + \Delta\lambda\Big(A_1\underline{n_1} + A_2\underline{n_2}\Big) = 0$

$R_\lambda = \Delta\lambda - \left\langle \frac{f}{K} \right\rangle^n \Delta t = 0$

$\underline{R_{\alpha_i}} = \Delta\underline{\alpha_i} - \Big(\underline{n_i} - \frac{D_i}{C_{ii}}(C_{ii}\underline{\alpha_i} + C_{ij}\underline{\alpha_j})\Big)\Delta\lambda + \left(\frac{2}{3}\right)^{m_i - 1} \frac{C_{ii}\underline{\alpha_i} + C_{ij}\underline{\alpha_i}}{J(C_{ii}\underline{\alpha_i} + C_{ij}\underline{\alpha_j})} \left\langle \frac{J(C_{ii}\underline{\alpha_i} + C_{ij}\underline{\alpha_j})}{M_i} \right\rangle^{m_i} \Delta t$

$R_{q_1} = \Delta q_1 - \Delta\lambda(1 - b_1 q_1)$

$R_{q_2} = \Delta q_2 - \Delta\lambda(1 - b_2 q_2)$

$R_q = \Delta q - \eta H(F) < \underline{n} : \underline{n}^* > \Delta\lambda$

$\underline{R_\xi} = \Delta\underline{\xi} - \sqrt{\frac{3}{2}}(1 - \eta)H(F) < \underline{n} : \underline{n}^* > \underline{n}^*\Delta\lambda$

In the previous system, the internal variables like $\underline{\alpha_i}$ are expressed as $\underline{\alpha_i}(t) + \theta\Delta\underline{\alpha_i}$, and the final system becomes complex. Jacobian matrix, solved at each Newton-Raphson iteration is built as shown in the following.

$$\begin{pmatrix} \underline{R_e} \\ R_\lambda \\ \underline{R_{\alpha_1}} \\ \underline{R_{\alpha_2}} \\ R_{q_1} \\ R_{q_2} \\ R_q \\ \underline{R_\xi} \end{pmatrix} = \begin{pmatrix} \frac{\partial R_e}{\partial \Delta \underline{\varepsilon_e}} & \frac{\partial R_e}{\partial \Delta \lambda} & \frac{\partial R_e}{\partial \Delta \underline{\alpha_1}} & \frac{\partial R_e}{\partial \Delta \underline{\alpha_2}} & \frac{\partial R_e}{\partial \Delta q_1} & \frac{\partial R_e}{\partial \Delta q_2} & \frac{\partial R_e}{\partial \Delta q} & \frac{\partial R_e}{\partial \Delta \underline{\xi}} \\ \frac{\partial R_\lambda}{\partial \Delta \underline{\varepsilon_e}} & \frac{\partial R_\lambda}{\partial \Delta \lambda} & \frac{\partial R_\lambda}{\partial \Delta \underline{\alpha_1}} & \frac{\partial R_\lambda}{\partial \Delta \underline{\alpha_2}} & \frac{\partial R_\lambda}{\partial \Delta q_1} & \frac{\partial R_\lambda}{\partial \Delta q_2} & \frac{\partial R_\lambda}{\partial \Delta q} & \frac{\partial R_\lambda}{\partial \Delta \underline{\xi}} \\ \frac{\partial R_{\alpha_1}}{\partial \Delta \underline{\varepsilon_e}} & \frac{\partial R_{\alpha_1}}{\partial \Delta \lambda} & \frac{\partial R_{\alpha_1}}{\partial \Delta \underline{\alpha_1}} & \frac{\partial R_{\alpha_1}}{\partial \Delta \underline{\alpha_2}} & \frac{\partial R_{\alpha_1}}{\partial \Delta q_1} & \frac{\partial R_{\alpha_1}}{\partial \Delta q_2} & \frac{\partial R_{\alpha_1}}{\partial \Delta q} & \frac{\partial R_{\alpha_1}}{\partial \Delta \underline{\xi}} \\ \frac{\partial R_{\alpha_2}}{\partial \Delta \underline{\varepsilon_e}} & \frac{\partial R_{\alpha_2}}{\partial \Delta \lambda} & \frac{\partial R_{\alpha_2}}{\partial \Delta \underline{\alpha_1}} & \frac{\partial R_{\alpha_2}}{\partial \Delta \underline{\alpha_2}} & \frac{\partial R_{\alpha_2}}{\partial \Delta q_1} & \frac{\partial R_{\alpha_2}}{\partial \Delta q_2} & \frac{\partial R_{\alpha_2}}{\partial \Delta q} & \frac{\partial R_{\alpha_2}}{\partial \Delta \underline{\xi}} \\ \frac{\partial R_{q_1}}{\partial \Delta \underline{\varepsilon_e}} & \frac{\partial R_{q_1}}{\partial \Delta \lambda} & \frac{\partial R_{q_1}}{\partial \Delta \underline{\alpha_1}} & \frac{\partial R_{q_1}}{\partial \Delta \underline{\alpha_2}} & \frac{\partial R_{q_1}}{\partial \Delta q_1} & \frac{\partial R_{q_1}}{\partial \Delta q_2} & \frac{\partial R_{q_1}}{\partial \Delta q} & \frac{\partial R_{q_1}}{\partial \Delta \underline{\xi}} \\ \frac{\partial R_{q_2}}{\partial \Delta \underline{\varepsilon_e}} & \frac{\partial R_{q_2}}{\partial \Delta \lambda} & \frac{\partial R_{q_2}}{\partial \Delta \underline{\alpha_1}} & \frac{\partial R_{q_2}}{\partial \Delta \underline{\alpha_2}} & \frac{\partial R_{q_2}}{\partial \Delta q_1} & \frac{\partial R_{q_2}}{\partial \Delta q_2} & \frac{\partial R_{q_2}}{\partial \Delta q} & \frac{\partial R_{q_2}}{\partial \Delta \underline{\xi}} \\ \frac{\partial R_q}{\partial \Delta \underline{\varepsilon_e}} & \frac{\partial R_q}{\partial \Delta \lambda} & \frac{\partial R_q}{\partial \Delta \underline{\alpha_1}} & \frac{\partial R_q}{\partial \Delta \underline{\alpha_2}} & \frac{\partial R_q}{\partial \Delta q_1} & \frac{\partial R_q}{\partial \Delta q_2} & \frac{\partial R_q}{\partial \Delta q} & \frac{\partial R_q}{\partial \Delta \underline{\xi}} \\ \frac{\partial R_\xi}{\partial \Delta \underline{\varepsilon_e}} & \frac{\partial R_\xi}{\partial \Delta \lambda} & \frac{\partial R_\xi}{\partial \Delta \underline{\alpha_1}} & \frac{\partial R_\xi}{\partial \Delta \underline{\alpha_2}} & \frac{\partial R_\xi}{\partial \Delta q_1} & \frac{\partial R_\xi}{\partial \Delta q_2} & \frac{\partial R_\xi}{\partial \Delta q} & \frac{\partial R_\xi}{\partial \Delta \underline{\xi}} \end{pmatrix} \begin{pmatrix} \Delta \underline{\varepsilon_e} \\ \Delta \lambda \\ \Delta \underline{\alpha_1} \\ \Delta \underline{\alpha_2} \\ \Delta q_1 \\ \Delta q_2 \\ \Delta q \\ \Delta \underline{\xi} \end{pmatrix}$$

Detailed expressions of the terms of the Jacobian matrix are presented in the appendix 1. Figures 9 et 10 compare the responses provided by the $2M1C$ model for the two kinds of local integration methods. The simulations were performed on the notched specimens previously defined and similar results were provided in this configuration (see Figure 9 et 10).

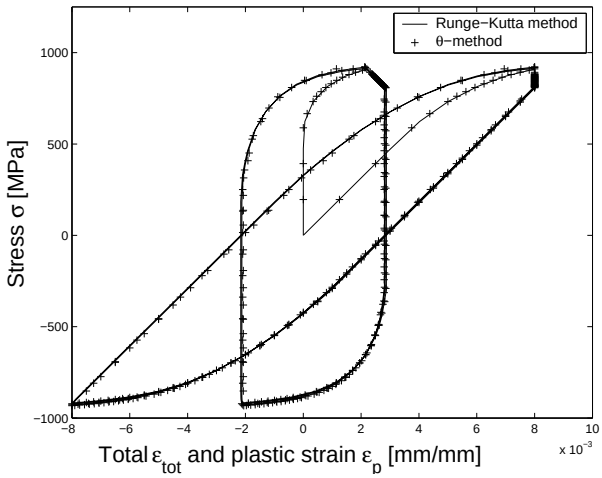

Figure 9. Comparison between explicit (Runge-Kutta) and implicit (θ-method) integration methods: stress-strain response

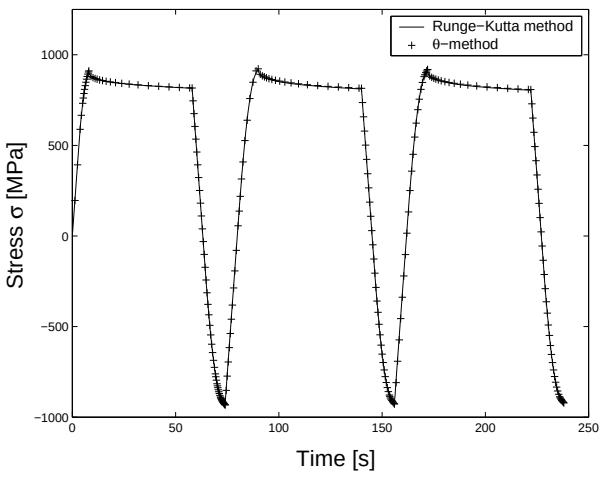

Figure 10. Comparison between explicit (Runge-Kutta) and implicit (θ-method) integration methods: stress-time response

4 Identification of the model parameters

Model parameter identification is based on pull-push tests (i.e in an unidirectional configuration) through a complexity growing multi-stage methodology.

4.1 One dimensional formulation

In this case, model formulation is simplified as following.

State laws (1) et (2) become:

$$\begin{array}{l|l} X_1 = C_{11}\alpha_1 + C_{12}\alpha_2 & R_1 = b_1 Q_1 q_1 \\ X_2 = C_{22}\alpha_2 + C_{12}\alpha_1 & R_2 = b_2 Q_2 q_2 \end{array}$$

Yield function has the following expression:

$$f = \sqrt{(\sigma_1 - X_1)^2 + (\sigma_2 - X_2)^2} - R_2 - R_1 - R_0$$

Evolution equations (3) et (4) can be written:

$$\begin{array}{l|l} \dot{\varepsilon_1} = \dot{\lambda}\frac{\sigma_1 - X_1}{\sqrt{(\sigma_1 - X_1)^2 + (\sigma_2 - X_2)^2}} & \dot{\varepsilon_2} = \dot{\lambda}\frac{\sigma_2 - X_2}{\sqrt{(\sigma_1 - X_1)^2 + (\sigma_2 - X_2)^2}} \\ \dot{\alpha_1} = \dot{\varepsilon_1} - \dot{\lambda}\frac{D_1}{C_{11}}X_1 - \left(\frac{|X_1|}{M_1}\right)^{m_1}\frac{X_1}{|X_1|} & \dot{\alpha_2} = \dot{\varepsilon_2} - \dot{\lambda}\frac{D_2}{C_{22}}X_2 - \left(\frac{|X_2|}{M_2}\right)^{m_2}\frac{X_2}{|X_2|} \\ \dot{q_1} = \dot{\lambda}\left(1 - \frac{R_1}{Q_1}\right) & \dot{q_2} = \dot{\lambda}\left(1 - \frac{R_2}{Q_2}\right) \end{array}$$

Last, the non-hardening region is described to take into account the memory effect (5) through the form:

$$F = |\varepsilon_{in} - \xi| - q; \qquad \dot{p} = |\dot{\varepsilon_{in}}| = |A_1\dot{\varepsilon_1} + A_2\dot{\varepsilon_2}|$$
$$\dot{q} = \eta H(F)\dot{\lambda}\langle \underline{n} : \underline{n}^* \rangle; \qquad \dot{\xi} = (1-\eta)H(F)sign(\varepsilon_{in} - \xi)\langle \underline{n} : \underline{n}^* \rangle\dot{\lambda}$$
$$\langle \underline{n} : \underline{n}^* \rangle = \langle sign(\varepsilon_{in} - \xi)(A_1(\sigma_1 - X_1) + A_2(\sigma_2 - X_2)) \rangle$$

4.2 Parameter identification

The identification process was performed with the SiDoLo™ optimization software (Pilvin (1998)). The process is divided in two main stages:

- First, the kinematic component intended to describe the fast evolution of the behavior, is determined with the type I test. After an initial strong softening, test sample reaches a quasi-stable stage (see figure 2), where the isotropic component may be assumed to be constant and equal to an apparent elastic limit R_0^*. From a modeling point of view, the tests with different strain rates allow the identification of the viscoplastic flow law (K,n) and the two kinematic hardening variables C_{ij} $(i, j = 1, 2)$. The kinematic coupling is able to describe the non-linearity of the hardening with only linear kinematic variables, the D_i $(i = 1, 2)$ dynamic recovery terms are fixed to zero. The viscous parameters are not sufficient to take into account the fatigue relaxation tests so as to reproduce the stress relaxation during dwell times which becomes very important at the high temperatures. Thus, static recovery terms are added in the kinematic variables m_i, M_i $(i = 1, 2)$. Last, the stress controlled tests are considered and all the cycles are included in the identification process. The localization parameters A_i $(i = 1, 2)$ of the two strain mechanisms are also determined from these cycles.

- In a second stage, the isotropic component of the model intended to reproduce the cyclic softening of the steel is considered. For that purpose, the first part of type I and type II tests are taken into account considering that the parameters identified previously remain fixed. Three terms are introduced: the first one R_1 (parameters $Q_{1\infty}$ and b_1) corresponds to the strong softening during the first hundred of cycles, the second one R_2 (parameters Q_2 and b_2) describes the continuous softening and the last one R_0 is the true elastic limit of the steel. Type II test is intended to verify that fixed parameters η and μ in the strain memory term are adequate.

Tables 7 and 8 provide the set of parameters identified for several temperature levels. Figures 11 to 16 show some identification results for different temperatures. Figures 16 and 17 compare experimental results and model responses for a continuous cycling and a several strain range cyclic softening with and without taking into account the plastic strain range memorization. In the last case (Figure 17), the model leads to a saturated cyclic softening after the first strain range level which is not observed from an experimental point of view. On the contrary, this phenomenom is reproduced by including the plastic strain range memrorization (Figure 16). This aspect was disccussed more deeply in previous works (Bernhart et al. (1999); Zhang et al. (2002)).

Table 7
55NiCrMoV7 kinematic parameters

		20° C	300° C	400° C	500° C
Kinematic parameters	$E(MPa)$	206580	188940	176580	156935
	R_0^*	500	420	330	270
	K	130	165	195	268
	n	19.5	18	17	15
	C_{11}	450480	406585	378675	195655
	D_1	0	0	0	0
	C_{22}	124980	91520	41965	13215
	D_2	0	0	0	0
	C_{12}	-149925	-126100	-84843	-40500
	A_1	0.78	0.74	0.66	0.65
	A_2	0.4	0.436	0.46	0.48
	M_1	795	760	740	705
	m_1	22	20	18	10.5
	M_2	890	850	800	700
	m_2	11.75	9.5	7	4.3

Table 8
55NiCrMoV7 isotropic parameters

		20° C	300° C	400° C	500° C
Isotropic param.	R_0	790	525	455	410
	$Q_{1\infty}$	-295	-80	-68	-100
	b_1	11	7	6	5.5
	Q_2	-75	-75	-75	-75
	b_2	0.2	0.2	0.2	0.2

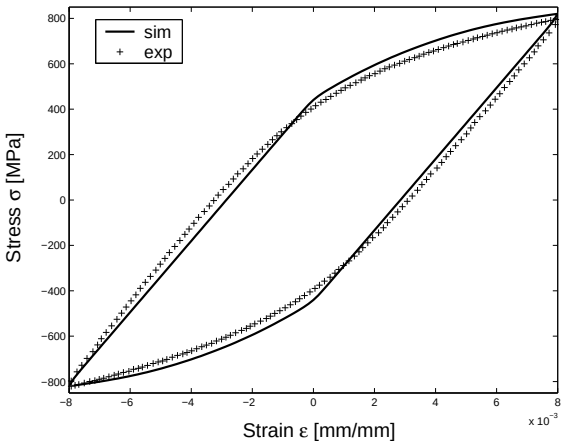

Figure 11. Comparison between experimental and calculated responses with a strain rate of $10^{-2}s^{-1}$ at a temperature of 500° C

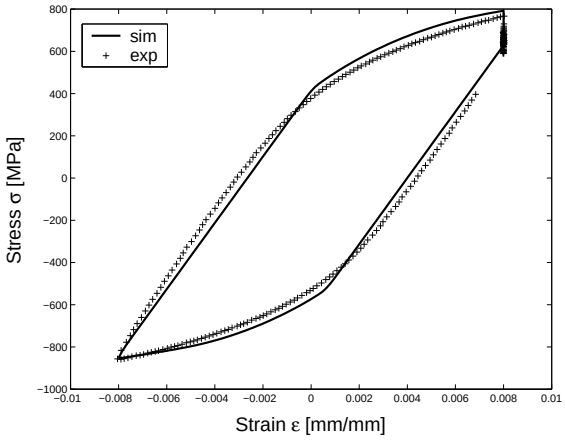

Figure 12. Comparison between experimental and calculated responses with a dwell time of $30s$ at a temperature of 500° C

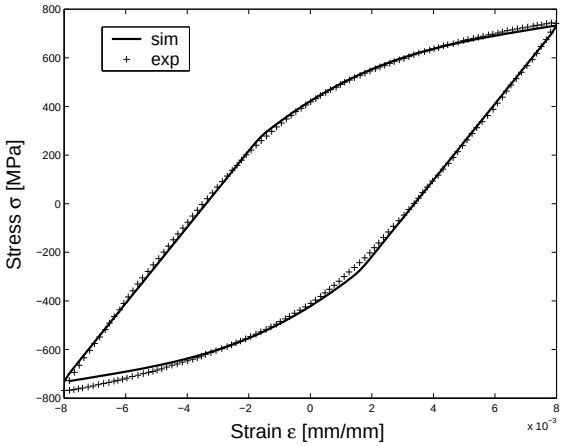

Figure 13. Comparison between experimental and calculated responses with a strain rate of $10^{-4}s^{-1}$ at a temperature of 500° C

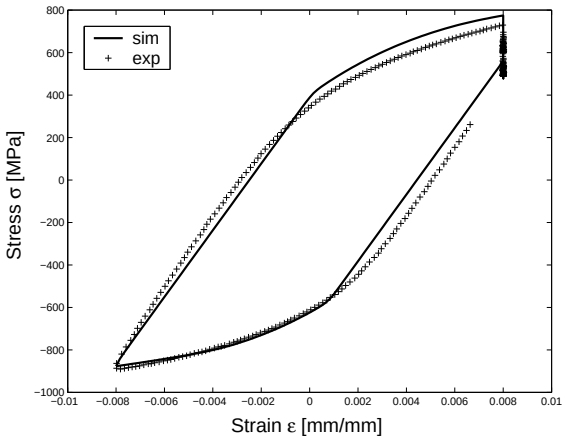

Figure 14. Comparison between experimental and calculated responses with a dwell time of $600s$ at a temperature of 500° C

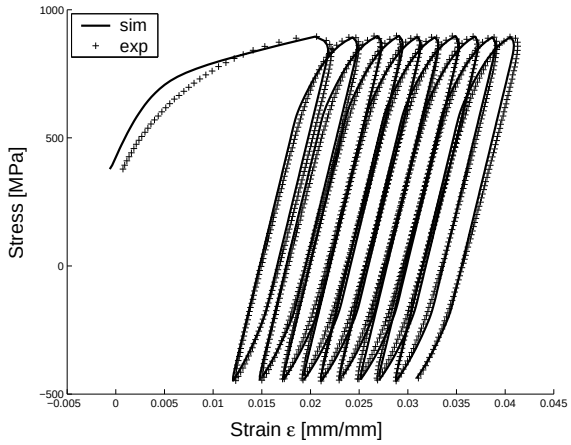

Figure 15. Comparison between experimental and calculated responses for a stress controlled test and a temperature of 500° C

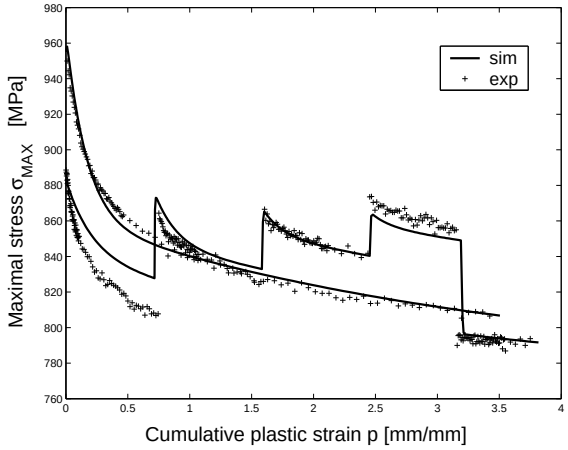

Figure 16. Comparison between experimental and calculated responses for a continuous and different strain range cyclic softening at 500° C with plastic strain range memorization

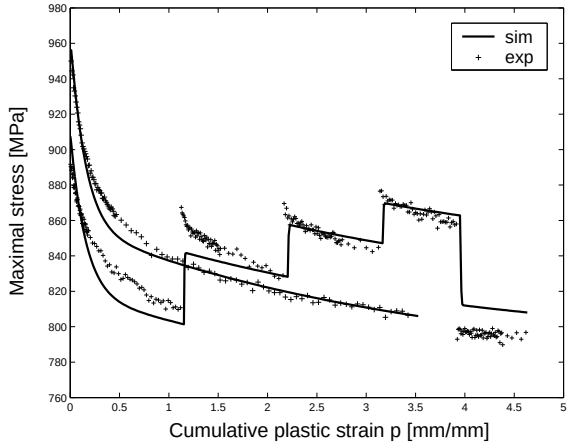

Figure 17. Comparison between experimental and calculated responses for a continuous and different strain range cyclic softening at 500° C without plastic strain range memorization

4.3 Discussion

4.3.1 Mathematical consideration

Multiplier identification:

The two strain mechanisms are associated to two localization coefficients A_1 and A_2. A careful examination of all the model equations allows to eliminate one of the two multipliers. Indeed, the one dimensional viscoplastic flow is written as:

$$\dot{\lambda} = \left\langle \frac{f}{K} \right\rangle^n \quad \text{with } f = \sqrt{(\sigma_1 - X_1)^2 + (\sigma_2 - X_2)^2} - R_0^*$$

if the apparent elastic limit of the material is considered when cyclic stabilization occurs.

As a consequence:

$$\sqrt{(A_1\sigma - X_1)^2 + (A_2\sigma - X_2)^2} = R_0^* + K\dot{\lambda}^{\frac{1}{n}}$$

and:

$$\sqrt{\left(\sigma - \frac{X_1}{A_1}\right)^2 + \left(\frac{A_2}{A_1}\sigma - \frac{X_2}{A_1}\right)^2} = \frac{R_0^*}{A_1} + \frac{K}{A_1}\dot{\lambda}^{1/n}$$

If the following assumptions are made:

$$\tilde{A} = \frac{A_2}{A_1}; \quad \tilde{C}_{11} = \frac{C_{11}}{A_1}; \quad \tilde{C}_{12} = \frac{C_{12}}{A_1}; \quad \tilde{C}_{22} = \frac{C_{22}}{A_1}; \quad \tilde{K} = \frac{K}{A_1}; \quad \tilde{R}_0^* = \frac{R_0^*}{A_1}$$

and:

$$\tilde{X}_1 = \frac{X_1}{A_1} = \tilde{C}_{11}\alpha_1 + \tilde{C}_{12}\alpha 2$$

$$\tilde{X}_2 = \frac{X_2}{A_1} = \tilde{C}_{12}\alpha_1 + \tilde{C}_{22}\alpha 2$$

we obtain:

$$\sqrt{(\sigma - \tilde{X}_1)^2 + (\tilde{A}\sigma - \tilde{X}_2)^2} = \tilde{K}\dot{\lambda}^{1/n} + \tilde{R}_0^*$$

In the general framework, the apparent elastic limit is replaced by the isotropic component and the previous equation can be written as:

$$\sqrt{(\sigma - \tilde{X}_1)^2 + (\tilde{A}\sigma - \tilde{X}_2)^2} = \tilde{K}\dot{\lambda}^{1/n} + \tilde{R}_1 + \tilde{R}_2 + \tilde{R}_0$$

with:

$$\tilde{R}_0 = \frac{R_0}{A_1}; \quad \tilde{R}_i = b_i\tilde{Q}_i q_i; \quad \tilde{Q}_i = \frac{Q_i}{A_1}; \quad i = 1, 2.$$

Consequently, no changes are introduced in the formulation by multiplying each parameter by the constant $1/A_1$ and, in this case, only one localization parameter has to be considered.

Non linear hardening description:

The coupling of the back stresses allows the description of the elastic-to-vicoplastic transition without any dynamic recovery terms. Indeed, if the most simple form of the model without any static term is considered, an analytical treatment of the evolution equations is possible. In this case, the one dimensionnal equations are written as:

$$\dot{\lambda} = \left\langle \frac{f}{K} \right\rangle^n$$
$$\sigma_1 = A_1\sigma; \quad \sigma_2 = A_2\sigma$$
$$X_1 = C_{11}\alpha_1 + C_{12}\alpha_2; \quad X_2 = C_{12}\alpha_1 + C_{22}\alpha_2$$
$$\dot{\alpha}_1 = \dot{\varepsilon}_1; \quad \dot{\alpha}_2 = \dot{\varepsilon}_2$$

If cyclic stabilization is considered,

$$R_v = R_0^* + K\dot{\lambda}^{1/n} = \sqrt{(A_1\sigma - X_1)^2 + (A_2\sigma - X_2)^2}$$

And finally, the following expression is obtained:

$$(A_1^2 + A_2^2)\sigma^2 - 2\sigma(A_1X_1 + A_2X_2) + X_1^2 + X_2^2 - R_v^2 = 0$$

Solutions of this equation are given by:

$$\sigma_i = \frac{(A_1X_1 + A_2X_2) \pm \sqrt{R_v^2(A_1^2 + A_2^2) - (A_1X_2 - A_2X_1)^2}}{A_1^2 + A_2^2}$$

Figure 18 compares the analytical response with experiment for a stabilized cycle at a strain rate equals to $10^{-2}s^{-1}$ and a temperature of $500^\circ\ C$.
It shows that, in such a coupled model formulation, non linear stress-strain curves can be obtained even if only linear kinematic hardening is considered.

4.3.2 Metallurgical consideration

The 2M1C model provides through the yield criterion two stress states induced by two different strain mechanisms which can be related to micro-structural evolutions

observed elsewhere. Indeed, the carbide coarsening and the decrease of the dislocation density are the main mechanisms inducing the cyclic softening of the tempered martensitic steel (Mébarki (2003)). The quenching generates a high dislocation density within the martensitic lathes. The cyclic load leads to an increase of the mean free motion of the dislocations. The rearrangement mechanism is the most important observed on the tempered martensitic steel (Mébarki (2003)). In the formulation, it is represented through the isotropic variable R_1 (and the strain mechanism ε_1) that describes the strong softening during the first hundred of cycles. The variable R_2 (and strain mechanism ε_2) represents the continuous linear softening and is attributed to the carbide coarsening mechanism. As a matter of fact, the increase of the test time induces a carbide coarsening which increases the dislocation free motion path and leads to a continuous softening.

The relative influence of these mechanisms on the cyclic softening amplitude was determined on a fatigue test performed at a temperature of 550° C, one third due to the carbide coarsening and two third due to the dislocation motion (Mébarki (2003)). A similar ratio was obtained with the 2M1C model, and such model seems to be an interesting tool to improve the knowledge of the micro-structural evolutions (see figure 19).

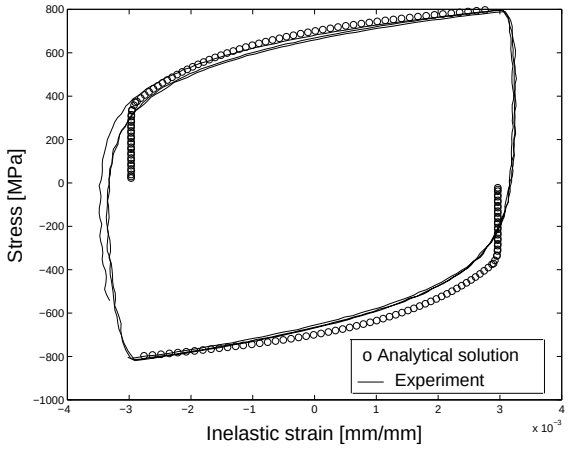

Figure 18. Comparison between the analytical solution and experiment for a strain rate of $10^{-2}s^{-1}$ (Stabilized cycle; T=500° C)

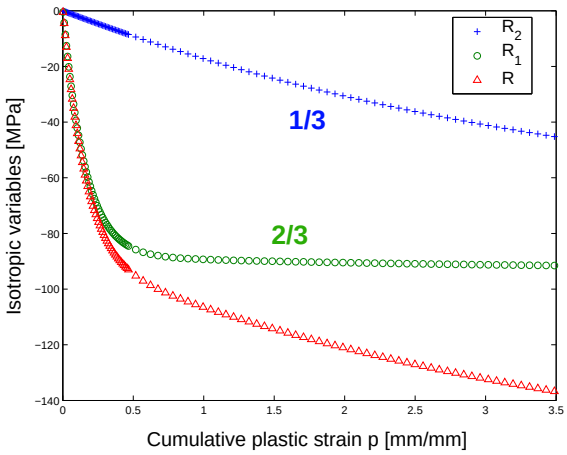

Figure 19. Simulation of the relative influence of the softening mechanisms for the 55NiCrMoV7 steel at 500° C

5 Isothermal Validation

5.1 Experimental and numerical procedure

In order to validate the model, two notched specimens were defined and several isothermal displacement and stress controlled tests were performed. Three different

extensometers were used (figure 20). The first one located at the centre of the specimen measures the radial displacement, the second one at 6 mm from the middle of the specimen the axial displacement, and the last one at 25 mm from the middle of the sample, is used to control the test. For the stress controlled tests, the load is applied at the upper part of the sample and stress is defined considering the surface S (figure 20). Displacement or stress block loadings are considered in the validation tests (table 9).

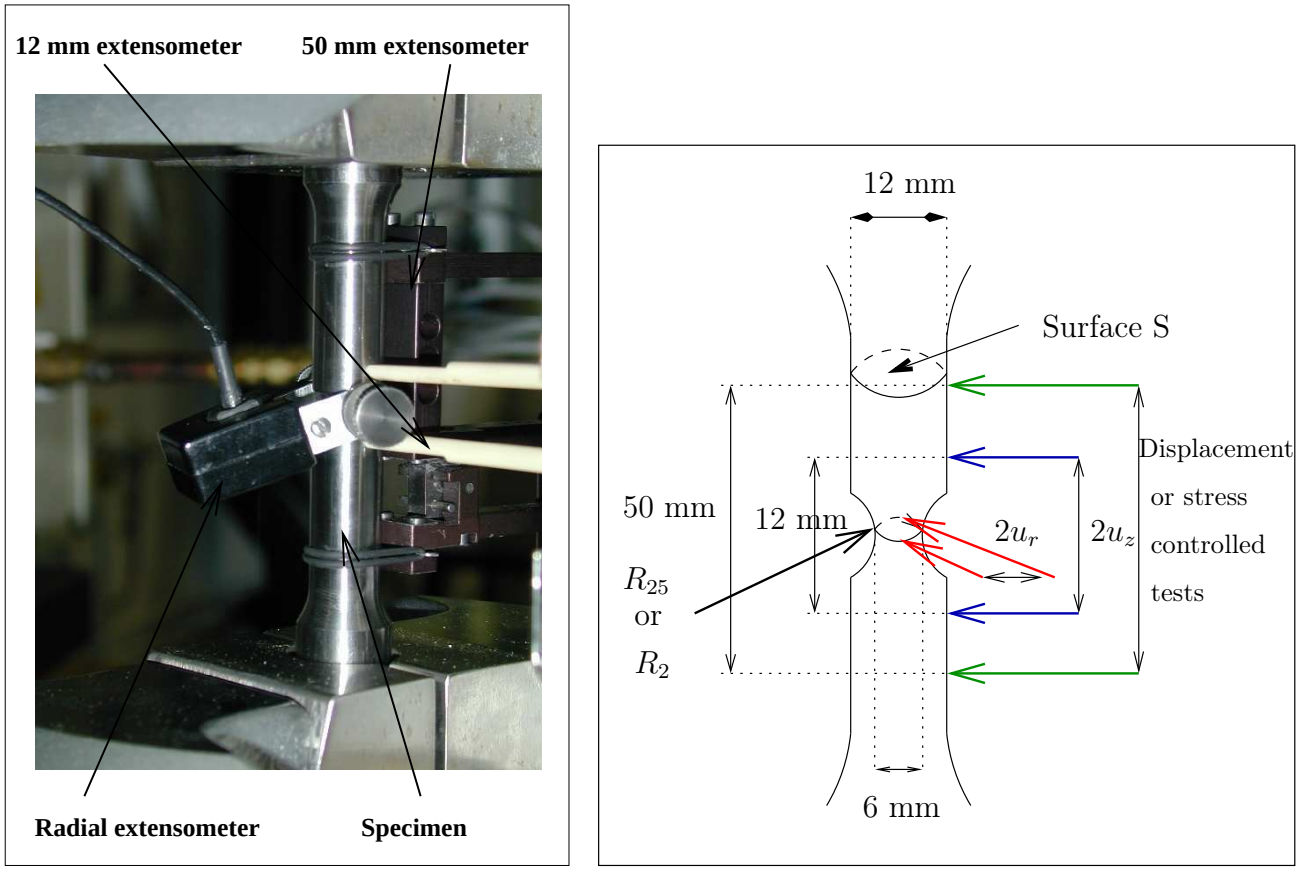

Figure 20. Extensometer locations on the specimen

Table 9
Validation tests performed on the notched specimens

Sample	strain or stress rate	loading levels (number of cycles)
R_{25}_STRESS	$\dot{\sigma} = 30\ MPa.s^{-1}$	+270/-135 MPa (6) ; +300/-150 MPa (14) ; +300/-200 MPa (5) ; +310/-155 MPa (11) ; +300/-260 MPa (8) ; +300/-300 MPa (4)
R_2_DISP	$\dot{\varepsilon} = 2.10^{-4}s^{-1}$	± 0.0375 mm (5); ± 0.05 mm (6); ± 0.05625 (6); ± 0.0625 mm (5); ± 0.05 mm (5); +0.0625/-0.05 mm (5); ± 0.06875 mm (4)

An axisymmetric finite element simulation is performed for both the specimens (figures 21 and 22) using ABAQUS™ software where the 2M1C model is implemented through the developer tool Z-Front (Zset package (1996)).

Two validation examples are illustrated in the next section, the first one concerns

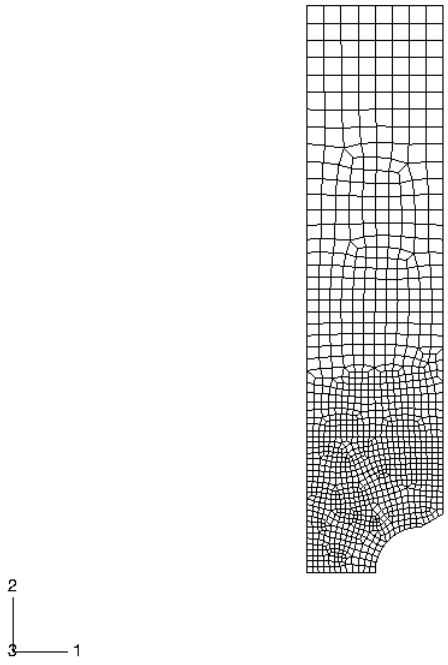

Figure 21. 2 mm notched specimen meshing

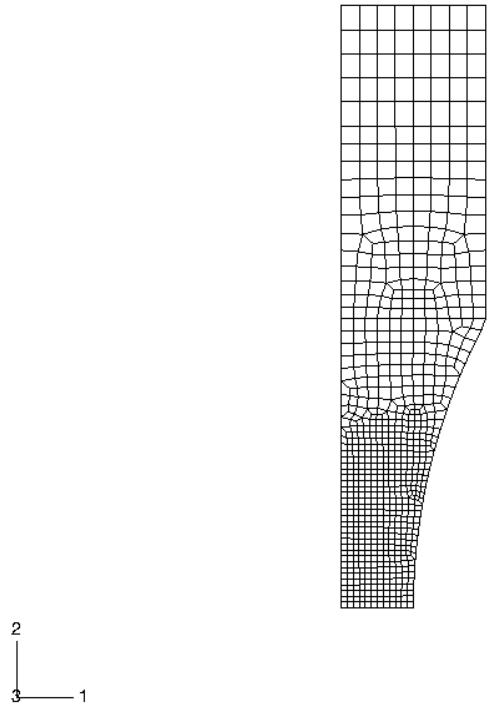

Figure 22. 25 mm notched specimen meshing

a displacement controlled test with seven load levels (figure 23), the second one represents a stress controlled test with six load levels (figure 24).

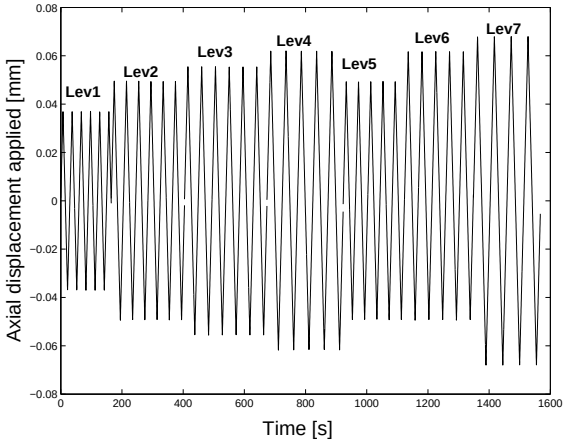

Figure 23. Displacement applied at the upper location of the specimen (25 mm from the centre)

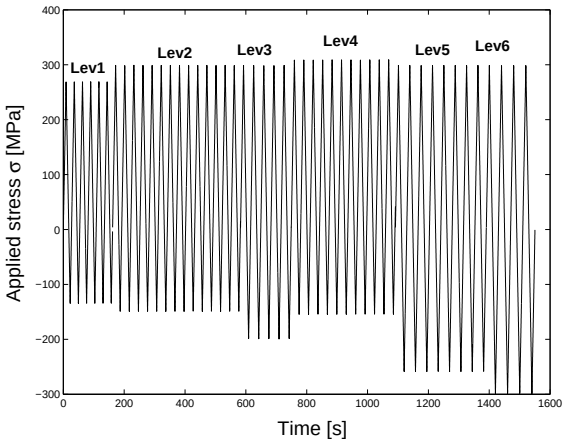

Figure 24. Stress applied at the upper location of the specimen (25 mm from the centre)

5.2 Validation results

5.2.1 Displacement controlled tests

Results provided by the 2M1C model are in a good agreement with the experimental ones for the axial and radial displacements and for the different loading levels as well.

The stress calculated at the upper part of the specimen is plotted versus the radial displacement for two levels (figures 25 and 26). They compare the numerical and experimental responses for the 2 mm notched specimen.

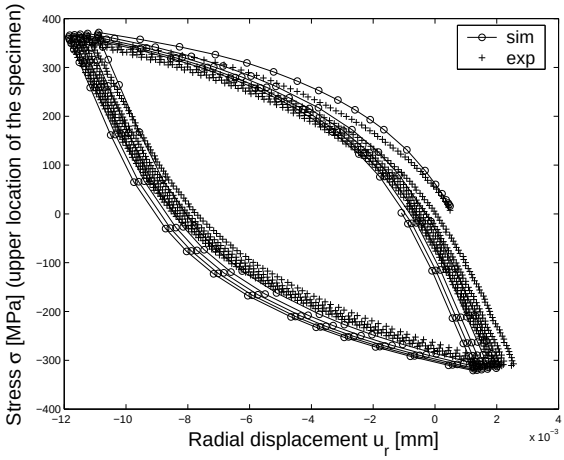

Figure 25. Comparison of the $\sigma - u_r$ experimental and calculated loop provided by the fifth loading level

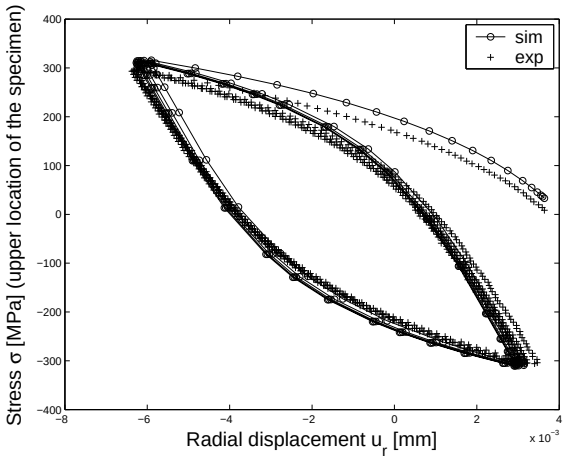

Figure 26. Comparison of the $\sigma - u_r$ experimental and calculated loop provided by the sixth loading level

Similar results were obtained for all the displacement controlled tests performed on the 2 mm and 25 mm notched specimens. It appears that the model capabilities to describe the behavior, are not affected by the geometry and the block loadings, even if the strain ranges reached at the centre of the specimens exceed those considered in the identification process ($\Delta\varepsilon = \pm 0.8\%$).

5.2.2 Stress controlled test

For the stress controlled tests, figures 27 and 28 compare the axial and radial displacements provided by the model with experiment for the 25 mm notched specimen. On the one hand, axial displacements are also well reproduced by numerical simulation whatever the test conditions and the specimen geometry. On the other hand, the radial displacements are not as well described as those in the axial direction. Several assumptions can be formulated to explain these differences:

- it could be a lack in the model parameter identification, indeed, only one level of stress range is considered and so only one mean stress value has been considered; this may be not sufficient to reproduce the ratcheting strain introduced by the validation tests where each block corresponds to a different mean stress value.
- from an experimental point of view, the radial measurements are difficult to implement. The extensometer is located at the centre of the specimen with two springs. However, the radial measurements performed for the displacement controlled tests have provided results in agreement with the calculated response. But, contrary to these ones, the stress controlled tests are characterized by an important non symmetry and a progressive sliding of the radial extensometer may appear. Optical measurements could be introduced in the future to avoid this possible perturba-

tion.

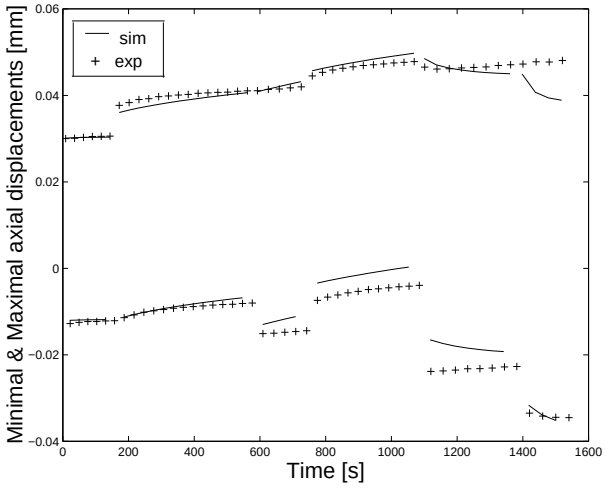

Figure 27. Comparison of the calculated and experimental axial displacement versus time

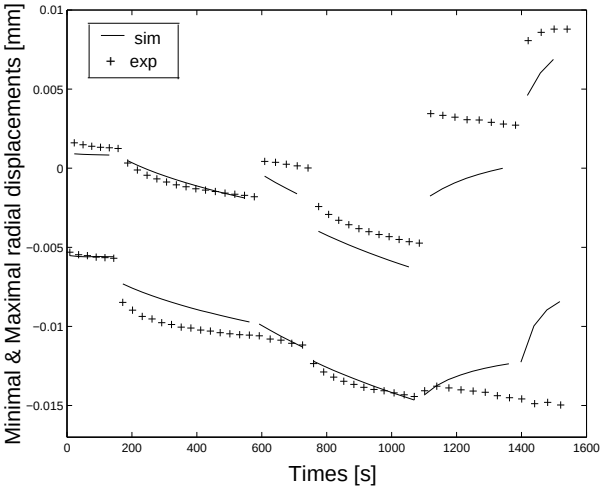

Figure 28. Comparison of the calculated and experimental radial displacement versus time

6 Conclusion

This work is a contribution to the description of the behavior of hot work tool steels. For that purpose, a methodology was implemented involving several stages. First, an automatic experimental process was defined in order to take into account the characteristic loadings to which tool steels are subjected. Indeed, the influence of the strain rate and strain range, of the dwell times within cycles as well as ratcheting or plastic accommodation effects for stress controlled tests, are included in the test procedure. The second part describes the 2M1C behavior model formulated in the framework of the irreversible process of thermodynamics. A detailed presentation of the three dimensional formulation was performed and the developments allowing the finite element implementation are provided. Hence, the 2M1C model was successfully identified by growing complexity level, according to the kinds of loads taken into account. It appears to be an interesting approach which provides a good description both of strain controlled and stress controlled tests. Moreover, the two different mechanisms included in the model were related to the micro-structural evolutions (dislocations and carbides) identified in low cycle fatigue. Last, a validation stage was performed on different notched specimens under displacement and stress controlled tests.

Acknowledgement: The authors gratefully acknowledge Denis Delagnes for many discussions related to the micro-structural evolutions of the tempered martensitic steels. The authors would like to express their sincere thanks to Professor Georges Cailletaud for the fruitfull discussions related to the 2M1C model formulation.

Appendix:

This part illustrates detailed calculations of the Jacobian matrix terms.

Term $\underline{R_e}$:

$$\frac{\partial \underline{n_i}}{\partial \underline{\sigma_i}} = \frac{\underline{\underline{I}} - \underline{n_i} \otimes \underline{n_i}}{\sqrt{J(\underline{\sigma_1} - \underline{X_1})^2 + J(\underline{\sigma_2} - \underline{X_2})^2}}$$

$$\frac{\partial \underline{n_i}}{\partial \underline{\sigma_j}} = -\frac{\underline{n_i} \otimes \underline{n_j}}{\sqrt{J(\underline{\sigma_1} - \underline{X_1})^2 + J(\underline{\sigma_2} - \underline{X_2})^2}} \qquad i \neq j, \quad i, j = 1, 2$$

$$\frac{\partial \underline{\underline{R_e}}}{\partial \Delta \underline{\varepsilon_e}} = \underline{\underline{I}} + \Delta\lambda \Big(A_1^2 \frac{\partial \underline{n_1}}{\partial \underline{\sigma_1}} + A_1 A_2 \frac{\partial \underline{n_1}}{\partial \underline{\sigma_2}} + A_1 A_2 \frac{\partial \underline{n_2}}{\partial \underline{\sigma_1}} + A_2^2 \frac{\partial \underline{n_2}}{\partial \underline{\sigma_2}} \Big) \underline{\underline{A}}$$

$$\frac{\partial \underline{\underline{R_e}}}{\partial \Delta \lambda} = A_1 \underline{n_1} + A_2 \underline{n_2}$$

$$\frac{\partial \underline{\underline{R_e}}}{\partial \Delta \underline{\alpha_i}} = -\frac{2}{3} \theta A_1 \Delta\lambda \Big(C_{ii} \frac{\partial \underline{n_1}}{\partial \underline{\sigma_i}} + C_{ij} \frac{\partial \underline{n_1}}{\partial \underline{\sigma_j}} \Big) - \frac{2}{3} \theta A_2 \Delta\lambda \Big(C_{ii} \frac{\partial \underline{n_2}}{\partial \underline{\sigma_i}} + C_{ij} \frac{\partial \underline{n_2}}{\partial \underline{\sigma_j}} \Big) \quad i = 1, 2 \; i \neq j$$

Term R_λ:

$$\frac{\partial R_\lambda}{\partial \Delta \underline{\varepsilon_e}} = -\theta \frac{n}{K} \Big\langle \frac{f}{K} \Big\rangle^{n-1} \Delta t \Big(A_1 \underline{n_1} + A_2 \underline{n_2} \Big) \underline{\underline{A}}$$

$$\frac{\partial R_\lambda}{\partial \Delta \lambda} = 1 + \Big\langle \frac{f}{K} \Big\rangle^{n-1} \frac{n}{K} \Delta t \theta (b_1 Q_1 e^{-b_1 \lambda} + b_2 Q_2 e^{-b_2 \lambda})$$

$$\frac{\partial R_\lambda}{\partial \Delta \underline{\alpha_i}} = \frac{2}{3} \theta \frac{n}{K} \Big\langle \frac{f}{K} \Big\rangle^{n-1} \Delta t \Big(C_{ii} \underline{n_i} + C_{ij} \underline{n_j} \Big) \quad i = 1, 2 \qquad i \neq j$$

$$\frac{\partial R_\lambda}{\partial \Delta q_i} = b_i \theta Q_i \frac{n}{K} \Big\langle \frac{f}{K} \Big\rangle^{n-1} \Delta t$$

$$\frac{\partial R_\lambda}{\partial \Delta q} = 2\mu b_1 q_1 \theta \Delta t \frac{n}{K} \Big\langle \frac{f}{K} \Big\rangle^{n-1} (Q_{1\infty} - Q_1)$$

Term $\underline{R_{\alpha_i}}$:

$$\frac{\partial \underline{\underline{R_{\alpha_i}}}}{\partial \Delta \underline{\varepsilon_e}} = -\Delta\lambda \Big(A_i \frac{\partial \underline{n_i}}{\partial \underline{\sigma_i}} + A_j \frac{\partial \underline{n_i}}{\partial \underline{\sigma_j}} \Big) \theta \underline{\underline{A}} \quad i, j = 1, 2 \quad i \neq j$$

$$\frac{\partial \underline{\underline{R_{\alpha_i}}}}{\partial \Delta \lambda} = -\Big(\underline{n_i} - \frac{D_i}{C_{ii}} \Big(C_{ii} \underline{\alpha_i} + C_{ij} \underline{\alpha_j} \Big) \Big); \quad i = 1, 2$$

$$\frac{\partial \Big(J(C_{ii} \underline{\alpha_i} + C_{ij} \underline{\alpha_j}) \Big)}{\partial \Delta \underline{\alpha_i}} = \frac{3}{2} \theta C_{ii} \frac{C_{ii} \underline{\alpha_i} + C_{ij} \underline{\alpha_j}}{J(C_{ii} \underline{\alpha_i} + C_{ij} \underline{\alpha_j})}$$

$$\frac{\partial \Big(J(C_{ii} \underline{\alpha_i} + C_{ij} \underline{\alpha_j}) \Big)}{\partial \Delta \underline{\alpha_j}} = \frac{3}{2} \theta C_{ij} \frac{C_{ii} \underline{\alpha_i} + C_{ij} \underline{\alpha_j}}{J(C_{ii} \underline{\alpha_i} + C_{ij} \underline{\alpha_j})}$$

$$\frac{\partial \underline{\underline{R_{\alpha_i}}}}{\partial \Delta \underline{\alpha_j}} = -\Big(\frac{\partial \underline{n_i}}{\partial \Delta \underline{\alpha_i}} - \frac{D_i}{C_{ii}} C_{ij} \theta \underline{\underline{I}} \Big) \Delta\lambda + \Big(\frac{2}{3} \Big)^{m_i - 1} \theta \frac{C_{ij} \underline{\underline{I}}}{J(C_{ii} \underline{\alpha_i} + C_{ij} \underline{\alpha_j})} \Big\langle \frac{J(C_{ii} \underline{\alpha_i} + C_{ij} \underline{\alpha_j})}{M_i} \Big\rangle^{m_i} \Delta t$$

$$- \theta\left(\frac{2}{3}\right)^{m_i-1}\frac{3}{2}\left\langle\frac{J(C_{ii}\underline{\alpha_i}+C_{ij}\underline{\alpha_j})}{M_i}\right\rangle^{m_i-1}\frac{C_{ij}}{J(C_{ii}\underline{\alpha_i}+C_{ij}\underline{\alpha_j})^3}(C_{ii}\underline{\alpha_i}+C_{ij}\underline{\alpha_j})\otimes(C_{ii}\underline{\alpha_i}+C_{ij}\underline{\alpha_j})\Delta t$$

$$+\frac{m_i}{M_i}\left(\frac{2}{3}\right)^{m_i-1}\frac{3}{2}\left\langle\frac{J(C_{ii}\underline{\alpha_i}+C_{ij}\underline{\alpha_j})}{M_i}\right\rangle^{m_i-1}\frac{\theta C_{ij}}{J(C_{ii}\underline{\alpha_i}+C_{ij}\underline{\alpha_j})^2}(C_{ii}\underline{\alpha_i}+C_{ij}\underline{\alpha_j})\otimes(C_{ii}\underline{\alpha_i}+C_{ij}\underline{\alpha_j})\Delta t;$$
$i \neq j$

$$\frac{\partial R_{\alpha_i}}{\partial\Delta\underline{\underline{\alpha_i}}} = \underline{\underline{I}} - \left(\frac{\partial\underline{\underline{n_i}}}{\partial\Delta\underline{\underline{\alpha_i}}} - D_i\theta\underline{\underline{I}}\right)\Delta\lambda + \left(\frac{2}{3}\right)^{m_i-1}\theta\frac{C_{ii}\underline{\underline{I}}}{J(C_{ii}\underline{\alpha_i}+C_{ij}\underline{\alpha_j})}\left\langle\frac{J(C_{ii}\underline{\alpha_i}+C_{ij}\underline{\alpha_j})}{M_i}\right\rangle^{m_i}\Delta t$$

$$-\frac{3}{2}\left(\frac{2}{3}\right)^{m_i-1}\theta\left\langle\frac{J(C_{ii}\underline{\alpha_i}+C_{ij}\underline{\alpha_j})}{M_i}\right\rangle^{m_i}\frac{C_{ii}}{J(C_{ii}\underline{\alpha_i}+C_{ij}\underline{\alpha_j})^3}(C_{ii}\underline{\alpha_i}+C_{ij}\underline{\alpha_j})\otimes(C_{ii}\underline{\alpha_i}+C_{ij}\underline{\alpha_j})\Delta t$$

$$+\frac{3}{2}\left(\frac{2}{3}\right)^{m_i-1}\theta\frac{m_i}{M_i}\left\langle\frac{J(C_{ii}\underline{\alpha_i}+C_{ij}\underline{\alpha_j})}{M_i}\right\rangle^{m_i-1}\frac{C_{ii}}{J(C_{ii}\underline{\alpha_i}+C_{ij}\underline{\alpha_j})^2}(C_{ii}\underline{\alpha_i}+C_{ij}\underline{\alpha_j})\otimes(C_{ii}\underline{\alpha_i}+C_{ij}\underline{\alpha_j})\Delta t;$$
$i = 1, 2$

$$\frac{\partial\underline{\underline{n_i}}}{\partial\Delta\underline{\underline{\alpha_i}}} = -\frac{2}{3}\theta\left(C_{ii}\frac{\partial\underline{\underline{n_i}}}{\partial\underline{\underline{\sigma_i}}} + C_{ij}\frac{\partial\underline{\underline{n_i}}}{\partial\underline{\underline{\sigma_j}}}\right) \quad i = 1, 2$$

$$\frac{\partial\underline{\underline{n_i}}}{\partial\Delta\underline{\underline{\alpha_j}}} = -\frac{2}{3}\theta\left(C_{ij}\frac{\partial\underline{\underline{n_i}}}{\partial\underline{\underline{\sigma_i}}} + C_{jj}\frac{\partial\underline{\underline{n_i}}}{\partial\underline{\underline{\sigma_j}}}\right) \quad i, j = 1, 2 \quad i \neq j$$

Term R_{q_i}:

$$\frac{\partial R_{q_1}}{\partial\Delta\lambda} = -(1 - b_1q_1)$$
$$\frac{\partial R_{q_1}}{\partial\Delta\lambda} = -(1 - b_2q_2)$$
$$\frac{\partial R_{q_1}}{\partial\Delta q_1} = 1 + b_1\theta\Delta\lambda$$
$$\frac{\partial R_{q_2}}{\partial\Delta q_2} = 1 + b_2\theta\Delta\lambda$$

Term R_q:

$$\frac{\partial\underline{\underline{n}}}{\partial\underline{\underline{\sigma}}} = A_1\frac{\partial\underline{\underline{n}}}{\partial\underline{\underline{\sigma_1}}} + A_2\frac{\partial\underline{\underline{n}}}{\partial\underline{\underline{\sigma_2}}}$$

$$\frac{\partial\underline{\underline{n}}}{\partial\underline{\underline{\sigma_i}}} = \frac{\sqrt{\frac{3}{2}}}{(D_n)^2}\left(\frac{2}{3}A_iD_n\underline{\underline{I}} - \left(A_1(\underline{\sigma_1}' - \underline{X_1}') + A_2(\underline{\sigma_2}' - \underline{X_2}')\right)\otimes\frac{\partial}{\partial\underline{\underline{\sigma_i}}}\left(D_n\right)\right)$$

$$\frac{\partial}{\partial\underline{\underline{\sigma_i}}}\left(D_n\right) = \frac{\frac{3}{2}A_i^2(\underline{\sigma_i}' - \underline{X_i}') + A_1A_2(\underline{\sigma_j}' - \underline{X_j}')}{D_n}; \qquad i \neq j$$

$$\frac{\partial R_q}{\partial\Delta\underline{\underline{\varepsilon_e}}} = -\eta H(F)\frac{\partial}{\partial\Delta\underline{\underline{\varepsilon_e}}}(<\underline{n} : \underline{n}^*>)\Delta\lambda$$

$$\frac{\partial}{\partial\Delta\underline{\underline{\varepsilon_e}}}(<\underline{n} : \underline{n}^*>) = \left(\underline{n}^*\frac{\partial\underline{\underline{n}}}{\partial\Delta\underline{\underline{\varepsilon_e}}} + \underline{n}\frac{\partial\underline{\underline{n}^*}}{\partial\Delta\underline{\underline{\varepsilon_e}}}\right)$$

$$\frac{\partial R_q}{\partial\Delta\lambda} = -\eta H(F) < \underline{n} : \underline{n}^* >$$

$$\frac{\partial R_q}{\partial\Delta\underline{\underline{\alpha_i}}} = \frac{2}{3}\theta\eta H(F)\Delta\lambda\underline{n}^*\left(C_{ii}\frac{\partial\underline{\underline{n}}}{\partial\underline{\underline{\sigma_i}}} + C_{ij}\frac{\partial\underline{\underline{n}}}{\partial\underline{\underline{\sigma_j}}}\right); \quad i = 1, 2; i \neq j$$

$$\frac{\partial R_q}{\partial\Delta q} = 1$$

$$\frac{\partial \underline{n}^*}{\partial \Delta \underline{\underline{\xi}}} = -\sqrt{\frac{3}{2}}\theta \frac{\underline{\underline{I}} - \underline{n}^* \otimes \underline{n}^*}{J(\underline{\varepsilon}_p - \underline{\xi})}$$

$$\frac{\partial R_q}{\partial \Delta \underline{\underline{\xi}}} = -\eta H(F) \Delta v \underline{n} \frac{\partial \underline{n}^*}{\partial \Delta \underline{\underline{\xi}}}$$

Term $\underline{R_\xi}$:

$$\frac{\partial R_\xi}{\partial \Delta \underline{\underline{\varepsilon_e}}} = -\sqrt{\frac{3}{2}}(1-\eta)H(F)\Delta\lambda\left(\underline{n}^* \otimes \left(\underline{n}^* \frac{\partial \underline{n}}{\partial \Delta \underline{\underline{\varepsilon_e}}}\right) + \underline{n}^* \otimes \left(\underline{n} \frac{\partial \underline{n}^*}{\partial \Delta \underline{\underline{\varepsilon_e}}}\right) + < \underline{n} : \underline{n}^* > \frac{\partial \underline{n}^*}{\partial \Delta \underline{\underline{\varepsilon_e}}}\right)$$

$$\frac{\partial R_\xi}{\partial \Delta \lambda} = -\sqrt{\frac{3}{2}}(1-\eta)H(F) < \underline{n} : \underline{n}^* > \underline{n}^*$$

$$\frac{\partial R_\xi}{\partial \Delta \underline{\alpha_i}} = \sqrt{\frac{2}{3}}(1-\eta)H(F)\Delta\lambda\theta\left(\underline{n}^* \otimes \left(\underline{n}^*\left(C_{ii}\frac{\partial \underline{n}}{\partial \underline{\sigma_i}} + C_{ij}\frac{\partial \underline{n}}{\partial \underline{\sigma_j}}\right)\right)\right) \quad i = 1, 2$$

$$\frac{\partial R_\xi}{\partial \Delta \underline{\underline{\xi}}} = \underline{\underline{I}} - \sqrt{\frac{3}{2}}(1-\eta)H(F)\left(\underline{n}^* \otimes \underline{n}\frac{\partial \underline{n}^*}{\partial \Delta \underline{\underline{\xi}}} + < \underline{n} : \underline{n}^* > \frac{\partial \underline{n}^*}{\partial \Delta \underline{\underline{\xi}}}\right)\Delta\lambda$$

References

Abbadi, M., Hähner, P., Zeghloul, A., 2002. On the characteristics of Portevin-Le-Chatelier bands in aluminium alloy 5182 under stress controlled and strain controlled tensile testing. Materials Science Engineering, 194–201.

Abdel-Karim, M., 2004. Numerical integration method for kinematic hardening rules with partial activation of dynamic recovery term. International Journal of Plasticity 21, 1303–1321.

Alfano, G., De Angelis, F., Rosati, L., 2001. General solution procedures in elasto-viscoplasticity. Computer Methods in Applied Mechanics and Engineering 190, 5123–5147.

Arnold, S., Saleeb, A., 1994. On the thermodynamic framework of generalized coupled thermoelastic-viscoplastic-damage modeling. International Journal of Plasticity 10 (3), 263–278.

Arnold, S., Saleeb, A., Castelli, M., 1996. A fully associative, non isothermal, nonlinear kinematic, unified viscoplastic model for titanium alloys. Thermomechanical Fatigue Behaviour and Materials 2.

Arnold, S., Saleeb, A., Wilt, T., 1995. A modeling investigation of thermal and strain induced recovery and nonlinear hardening in potential based viscoplasticity. Journal of Engineering Materials and Technology 117, 157–167.

Bari, S., Hassan, T., 2000. Anatomy of coupled constitutive models for ratcheting simulation. International Journal of Plasticity 16, 381–409.

Bari, S., Hassan, T., 2001. Kinematic hardening rules in uncoupled modeling for multiaxial ratcheting simulation. International Journal of Plasticity 17, 885–905.

Bari, S., Hassan, T., 2002. An advancement in cyclic plasticity modeling for multiaxial ratcheting simulation. International Journal of Plasticity 18, 873–894.

Ben Cheikh, A., 1987. Elastoviscoplasticité à température variable. Ph.D. thesis, Université de Paris 6, in French.

Benallal, A., 1990. Validation of structural computation codes in elastoviscoplasticity. International Journal for Numerical Methods in Engineering 29, 1109–1130.

Benallal, A., Marquis, D., 1987. Constitutive equations for non proportional cyclic elastoviscoplasticity. Journal of Engineering Materials and Technology 109, 326–336.

Bernhart, G., Moulinier, G., Brucelle, O., Delagnes, D., 1999. High temperature low cycle behaviour of martensitic forging tool steel. International Journal of Fatigue 21 (2), 179–186.

Blaj, L., Cailletaud, G., 2000. Application of a multimechanism model to the prediction of ratcheting behavior. In: SF2M (Ed.), Advances in Mechanical Behaviour, Plasticity and Damage. Vol. 2. pp. 1155–1160.

Bodner, S., 1987. A review of an unified elasto-viscoplastic theory, unified constitutive equations for creep and plasticity. London: Elsevier Applied Science.

Cailletaud, G., Forest, S., Jeulin, D., Feyel, F., Galliet, I., Mounoury, V., Quilici, S., 2003. Some elements of microstructural mechanics. Computational Materials Science 27, 351–374.

Cailletaud, G., Sai, K., 1995. Study of plastic/viscoplastic models with various inelastic mechanisms. International Journal of Plasticity 11, 991–1005.

Chaboche, J., 1986. Time independent constitutive theories for cyclic plasticity. International Journal of Plasticity 2 (2), 149–188.

Chaboche, J., 1987. Cyclic plasticity modeling and ratcheting effects. In: 2° International conference on constitutive laws for engineering materials: theory and applications. Tucson, Arizona, Desai et al, Elsevier, pp. 47–58.

Chaboche, J., 1989. Constitutive equations for cyclic plasticity and cyclic viscoplasticity. International Journal of Plasticity 5, 247–302.

Chaboche, J., Dang-Van, K., Cordier, G., 1979. Modelization of the strain memory effect on the cyclic hardening of 316 stainless steel. In: SMIRT-5 Division L., Berlin. pp. 13–17.

Chaboche, J., Nouailhas, D., Pacou, D., Paulmier, P., 1991. Modeling of the cyclic response and ratcheting effects on inconel 718 alloy. European Journal of Mechanic, A/solids 10 (1), 101–121.

Chan, K., Bodner, S., Lindholm, U., 1988. Phenomenological modeling of hardening and thermal recovery in metals. Journal of Engineering Materials and Technology 110, 1–8.

Chen, X., Jiao, R., 2004. Modified kinematic hardening rule for multiaxial ratcheting prediction. International Journal of Plasticity 20, 871–898.

Chen, X., Jiao, R., Kim, K., 2005. On the Ohno-Wang kinematic hardening rules for multiaxial ratcheting modeling of medium carbon steel. International Journal of Plasticity 21, 161–184.

Colak, O., 2004. A viscoplasticity theory applied to proportional and non-proportional cyclic loading at small strains. International Journal of Plasticity 20, 1387–1401.

Contesti, E., Cailletaud, G., 1989. Description of creep-plasticity interaction with non-unified constitutive equations application to an austenitic stainless steel. Nuclear Engineering Design 116 (3), 265–280.

Corona, E., Hassan, T., Kyriakides, S., 1996. On the performance of kinematic hard-

ening rules in predicting a class of biaxial ratcheting histories. International Journal of Plasticity 12 (1), 117–145.

Delagnes, D., 1998. Isothermal fatigue behaviour and lifetime of 5% Cr hot work tool steel around the LCF-HCF transition. Ph.D. thesis, Ecole Nationale Supérieure des Mines de Paris, in French.

Dieng, L., Abdul-Latif, A., Haboussi, M., Cunat, C., 2005. Cyclic plasticity modeling with the distribution of non linear relaxations approach. International Journal of Plasticity 21, 353–379.

Duvaut, G., 1990. Mécanique des Milieux Continus. Masson, Paris, in French.

Döring, R., Hoffmeyer, J., Seeger, T., Vormwald, M., 2003. A plasticity model for calculating stress-strain sequences under multiaxial non proportional cyclic loading. Computational Materials Science 28, 587–596.

Eberl, F., Feyel, F., Quilici, S., Cailletaud, G., 1998. Approches numériques de la plasticité cristalline. Journal of Physics IV 8, in French.

Estrin, Y., 1991. A versatile unified constitutive model based on dislocation density evolution. High Temperature Constitutive Modeling - Theory and Application 121, 65–83.

Estrin, Y., 1996. Dislocation-density-related constitutive modeling. Unified Constitutive Laws of Plastic Deformation, Academic Press.

Estrin, Y., Braasch, H., Brechet, Y., 1996. A dislocation density based constitutive model for cyclic deformation. Journal of Engineering Materials and Technology 118, 441–447.

Flouriot, S., Forest, S., Rémy, L., 2003. Strain localization phenomena under cyclic loading: application to fatigue of single crystals. Computational Materials Science 26, 61–70.

Foerch, R., 1996. An object-oriented environment for the numerical modeling materials and structural calculations. Ph.D. thesis, Ecole Nationale Supérieure de Mines de Paris.

Foerch, R., Gros, V., Mounoury, V., Quilici, S., Cailletaud, G., 2000. Cyclic calculations and life prediction in thermomechanical fatigue using the zmat library. In: ABAQUS Users' Conference, Newport, Rhode Island. pp. 289–304.

Forest, S., Cailletaud, G., 1995. Strain localization in single crystals: bifurcation analysis, effects of boundaries and interfaces. European Journal of Mechanics, A/Solids 14 (5), 747–771.

Germain, P., Muller, P., 1995. Introduction à la mécanique des milieux continus. Masson, 2° édition, in French.

Gomez, V., 2002. Etude en fatigue biaxiale à haute température d'alliages métalliques pour disques de turbomachines aéronautiques. Ph.D. thesis, Université Paul Sabatier Toulouse 3, in French.

Halphen, B., Nguyen, Q., 1974. Plastic and viscoplastic materials with generalized potential. Mechanics Research Communication 1 (1), 43–47.

Lemaître, J., Benallal, A., Marquis, D., 1992. Lifetime prediction of structures in anisothermal viscoplasticity coupled to damage. Nuclear Engineering and Design 133, 346–360.

Lemaître, J., Chaboche, J., 1994. Mechanics of solid materials. Cambridge University Press.

Malinin, N., Khadjinsky, G., 1972. Theory of creep with anisotropic hardening. International Journal of Mechanics and Sciences 14, 235–246.

Miller, A., 1976. An inelastic constitutive model for monotonic cyclic and creep deformation: Equations development and analytical procedures. Journal of Engineering Materials and Technology, 97–105.

Mébarki, N., 2003. Relationship between microstructure and mechanical properties of tempered martensitic steel. Ph.D. thesis, Ecole Nationale Supérieure des Mines Paris, in French.

Méric, L., Cailletaud, G., 1991a. Single crystal modeling for structural calculations:part 1- model presentation. Journal of Engineering Materials and Technology 113, 171–182.

Méric, L., Cailletaud, G., 1991b. Single crystal modeling for structural calculations:part 2- finite element implementation. Journal of Engineering Materials and Technology 113, 171–182.

Nicouleau, E., Feyel, F., Quilici, S., Cailletaud, G., 2001. Structural calculations and life prediction in thermomechanical fatigue of industrial components. In: Temperature-Fatigue Interaction. 9^{th} International Spring Meeting (Paris), pp. 363–372.

Nouailhas, D., Culié, J., Cailletaud, G., Méric, L., 1995. Finite element analysis behavior of single-crystal tubes. European Journal of Mechanics A/Solids 14 (1), 137–154.

Nouailhas, D., Policella, H., Kaczmarek, H., 1983. On the description of cyclic hardening under complex loading histories. In: International Conference on Constitutive Laws for Engineering Materials. Tucson, Arizona, Desai et al, Elsevier, pp. 45–49.

Ohno, N., 1982. A constitutive model of cyclic plasticity with a non hardening strain region. Journal of Applied Mechanics 49, 721–727.

Ohno, N., Wang, J., 1991. Transformation of a nonlinear kinematic hardening rule to a multisurface form under isothermal and nonisothermal conditions. International Journal of Plasticity 7, 879–891.

Ohno, N., Wang, J., 1993. Kinematic hardening rules with critical state of dynamic recovery, parts I and II. International Journal of Plasticity 9, 375–403.

Pilvin, P., 1998. SiDoLo version 2.4.

Portier, L., Calloch, S., Marquis, D., Geyer, P., 2000. Ratchetting under tension-torsion loadings experiments and modelling. International of Plasticity 16, 303–335.

Quilici, S., Cailletaud, G., 1999. FE simulation of macro-, meso- and micro-scales in polycristalline plasticity. Computational Materials Science 16, 383–390.

Samrout, H., Abdi, R. E., 1997. Model for 28CrMoV5-8 steel undergoing thermomechanical cyclic loadings. International Journal of Structures 34 (35-36), 4547–4556.

Schmidt, C., Miller, A., 1981. An unified phenomenological model for non-elastic deformation of type 316 l stainless steel. Research Mechanica 3, Part I: 109–129; Part II: 129–175.

Simo, J., Taylor, R., 1985. Consistent tangent operators for rate-independent elastoplasticity. Computer Methods in Applied Mechanics and Engineering 48, 101–118.

Vincent, L., Calloch, S., Marquis, D., 2004. A general cyclic plasticity model tak-

ing into account yield surface distortion for multiaxial ratcheting. International Journal of Plasticity 20, 1817–1850.

Voyiadjis, G., Al-Rub, R. A., 2003. Thermodynamic based model for the evolution equation of the backstress in cyclic plasticity. International Journal of Plasticity 19, 2121–2147.

Voyiadjis, G., Al-Rub, R. A., Palazotto, A., 2004. Thermodynamic framework for coupling of non-local viscoplasticity and non-local anisotropic viscodamage for dynamic localization problems using gradient theory. International Journal of Plasticity 20, 981–1038.

Wang, J., Ohno, N., 1991. Two equivalent forms of nonlinear kinematic hardening: Application to non isothermal plasticity. International Journal of Plasticity 7, 637–650.

Xu, B., Jiang, Y., 2004. A cyclic plasticity model for single crystals. International Journal of Plasticity 20, 2161–2178.

Yaguchi, M., Yamamoto, M., Ogata, T., 2002a. A viscoplastic constitutive model for nickel-base superalloy, part 1: kinematic hardening rule of anisotropic dynamic recovery. International Journal of Plasticity 18, 1083–1109.

Yaguchi, M., Yamamoto, M., Ogata, T., 2002b. A viscoplastic constitutive model for nickel-base superalloy, part 2: modeling under anisothermal conditions. International Journal of Plasticity 18, 1111–1131.

Zhang, Z., 2002. Anisothermal cyclic behaviour modeling with taking account of tempering effect of a martensitic tool steel 55NiCrMoV7. Ph.D. thesis, Ecole Nationale Supérieure des Mines de Paris, in French.

Zhang, Z., Delagnes, D., Bernhart, G., 2002. Anisothermal cyclic plasticity modeling of martensitic steels. International Journal of Fatigue 24, 635–648.

Zset package, 1996. User and developer manuals. http://www.nwnumerics.com, http://www.mat.ensmp.fr.